Numerical study on propulsion of flapping flight at low Reynolds number

Bachelor thesis

UNIVERSIDAD CARLOS III DE MADRID
Escuela Politécnica Superior

Aerospace engineering degree
Dpto. de Bioingeniería e Ingeniería aeroespacial

Author:
Lara Díaz López

Director:
Manuel Moriche Guerrero

Leganés, September 2017

Abstract

Along the history, innumerable studies about the kinematics that govern flapping flight at high Reynolds number can be found. Although the literature of this kind of flight at low Reynolds number is also huge, the unsteadiness in the aerodynamics, is still really complex to predict due to the amount of parameters involved in it.

This bachelor thesis aims to study the best configuration of parameters involved in the kinematics of a flapping airfoil, to achieve the maximum propulsive efficiency and thrust as possible, without penalizing the generated lift.

To make the study possible, the Navier Stokes equations, for an incompressible flow around an airfoil, are solved by means of Direct Numerical Simulations, where an Immersed Boundary Method is implemented.

In the process 48 cases are simulated. The immersed body selected is a NACA 0012 profile. Due to the unmanageable number of parameters that affects to the kinematics of the problem, some of them are kept fixed while other varies. A Reynolds number of $Re = 500$, a reduced frequency of $k = 1.41$, a phase shift between pitching and heaving of $\varphi = 90^o$ and a heaving amplitude of $h/c = 1$ are selected. Feathering parameter (χ) is going to be studied in the range of values between 0 and 1, where propulsive forces appears. The selected values of χ have their associated values of pitching amplitude (θ_0) and the mean pitch angle (θ_m) is adjusted according to the equations of motion to achieved some desired values of mean lift coefficient in the range of values between 0 and 1.5. It is observed, how at $\chi \simeq 0.5$ maximum values of thrust are obtained while at $\chi \simeq 0.7$ maximum values of propulsive efficiency are achieved.

Moreover, it is included a comparison of the results obtained in the actual project with the ones of a companion project (Yuste 2017).

Acknowledgement

First of all, I would like to express my most sincere gratitude to my supervisor, Prof. Manuel Moriche Guerrero, who has supported me along the development of this bachelor thesis with his continuous advice, knowledge, patience and motivation. Also, my deepest gratitude to Prof. Manuel García Villalba for trusting me, and giving me the opportunity of learning more from the aerospace and bioengineering department, and Prof. Óscar Flores for his advice.

I want to thank all my classmates for the support along the years, specially to my girls that have become more than classmates and with whom I have spent most of these years, that I will remember for the good times.

Last but not least, I can not be more grateful to my parents, for their unconditional support and love, for trusting me when I did not even do it, and for their guidance along my life. I can not forget my little sister, I will always be thankful for having her in my life. Thanks to Adri for making these years better. Without them this would not be possible.

Glossary

α_e	Effective angle of attack
χ	Feathering parameter
Δt	Time step
ΔV	Associated volume to a lagrangian marker
Δx	Mesh width in x direction
Δz	Mesh width in z direction
Γ	Total circulation of the flow
Γ_T	Translational circulation
Γ_R	Rotational circulation
ρ	Density of the fluid
μ	Kinematic viscosity
ν	Dynamic viscosity
φ	Phase shift
θ	Angular displacement of pitching motion
$\dot{\theta}$	Angular velocity of pitching motion
θ_0	Pitching amplitude
θ_m	Mean pitch angle
ω	Angular velocity
$\vec{\omega}$	Vorticity field vector
ϕ	Potential of the flow
b	Span of the wing
c	Chord of the airfoil
c_l	Non- dimensional drag coefficient per unit length. $c_d = \frac{2F_x}{\rho U_\infty^2 c}$
c_l	Non- dimensional lift coefficient per unit length. $c_l = \frac{2F_z}{\rho U_\infty^2 c}$
c_t	Non- dimensional thrust coefficient per unit length. $c_t = \frac{-2F_x}{\rho U_\infty^2 c}$

e_x	Unitary vector in x direction
e_z	Unitary vector in z direction
f	Frequency of oscillation
G_T	Translational coefficient in quasi-steady model for circulation
G_T	Rotational coefficient in quasi-steady model for circulation
h	Vertical displacement of heaving motion
$\dot{h}$	Vertical velocity of heaving motion
h_0	Heaving amplitude
k	Reduced frequency $k = 2\pi fc/U_\infty$
F_x	Force per unit length in x direction
F_z	Force per unit length in z direction
$M_{y,c/4}$	Pitching moment per unit length at c/4 of the leading edge
$\vec{n}$	Unitary normal vector pointing towards the fluid
n_{steps}	Number of steps per period
N_x	Number of grid points in x direction
N_z	Number of grid points in z direction
$p.c$	Number of points per chord
Re	Reynolds number $Re = U_\infty c/\nu$
St	Strouhal number $St = fc/U_\infty$
t	Time
T	Period
U_∞	Free stream velocity
W	Mechanical work
x	Stream-wise direction axis
x_0	Initial coordinate of the computational domain in x direction
x_f	Final coordinate of the computational domain in x direction
x_p	Distance from the leading edge to the pivoting point
z	Vertical direction axis
z_0	Initial coordinate of the computational domain in z direction
z_f	Final coordinate of the computational domain in z direction

Acronyms

2D	Two Dimensional
AR	Aspect Ratio
BC	Boundary Conditions
CFD	Computational Fluid Dynamics
CFL	Courant Fredrich Levy number
DARPA	Defense Advanced Research Project Agency
DNS	Direct Numerical Simulation
HDF5	Hierarchical Data Format version 5
IBM	Immersed Boundary Method
I/O	Input/Output tasks
LE	Leading Edge
LEV	Leading Edge Vortex
MAV	Micro Air Vehicle
MPI	Message Parsing Interface
NACA	National Advisory Commitee dor Aeronautics
TE	Trailing Edge
TEV	Trailing Edge Vortex
TUCAN	Two(Three)- Dimensional Unsteady Code for Aerodynamics in Nature

List of Tables

List of Figures

Contents

Chapter 1

Introduction

1.1 Motivation

Since the beginning of the time, although more concretely since the human being starts to develop his knowledge about the things that takes place around him, humans have been interested in how birds and insects could fly. Although the first prototype of a flying machine imitating the wings of birds was made by Leonardo Da Vinci on the 16th century, the interest of humans in these machines would increase on the 17th century once Issac Newton discovers and explains the gravitational laws that actuate in our planet. With the development of knowledge and thus, the advance in technology, the first manned flights that challenges these laws takes place on the 19th century, thanks to Otto Lilienthal creator of hang gliders, but it will be on the 20th century when the Wright brothers made possible the first successful flight in history with a machine heavier than the air, that allows to cover 120 feet in 12 seconds. Since then, the aeronautical industry has lived significant changes passing from the simplest powered aircraft, to rotary-wing aircraft or supersonic aircraft which nowadays are still in development to allow the possibility of cover huge distances in civil flights. Nevertheless, although the tendency in the past century has been the development of bigger and faster aircraft with and associated growth in Reynolds number, that has evolved from a $Re \simeq 3 \cdot 10^6$ in 1903 with the flight of the Wright brothers to $Re \simeq 7 \cdot 10^7$ in 1977 with the launching of the Concorde, in the past decades the interest in lighter and efficient machines has increased as well as the interest in Micro Air Vehicles (MAV) that tries to imitate the performance of birds and insects whose Reynolds number is much smaller than the ones cited.

MAVs have been defined by the Defense Advanced Research Project Agency (DARPA) as micro aerial vehicles for having dimensions no larger than 15 cm. These flying vehicles have attracted the interest of the industry for its huge variety of applications since they are used for commercial and research purposes, they can access easily to hidden uneven places, for humanitarian or military missions and they are equipped with sensors that allow to perform reconnaissance, surveillance and testing activities in hazardous and remote places. Since MAVs have been developed imitating the performance of small birds and insects, they

fly at Reynolds numbers of the order of 10 to 10^4, so that the flow separation at the boundary layer and the transition between the laminar and turbulent regime, behaves differently than in conventional aircraft built until now, taking special importance the airfoil shape that affects the performance of these aerial vehicles. MAVs are able to reach cruising velocities between 10 m/s to 20 m/s in a flying motion characterized by high amplitudes and moderate frequencies, (Shyy et al. 2013), and due to their small shape and light weight, they are prone to be sensitive to the wind gusts that take place suddenly in the in the flow, although these physical characteristics of MAVs have not penalized their structural strength.

Although MAVs have attract the aeronautical interest into the study of the unsteady aerodynamics of flapping wings, this is a complex and challenging subject to dominate due to the huge number of parameters that affect to it. Thus, simplified models are used to study how some kinematic parameters affect the aerodynamic forces and moments. To make this possible the natural movements of birds and insects are imitated to achieve the most effective performance in this kind of vehicles. Until now, conventional aircraft have been equipped with ailerons that generate similar twisting moment as the ones that birds produce naturally with their wings. Nevertheless, this movement is more complex and takes place by a combination of pitching movement respect to their spanwise axis, located along their wings and a rotation about the wing to body union. The task of reproducing a structure, to recreate these movements with the required flexibility, taking into account all the parameters that can affect to it, becomes a challenging task. Moreover, the study of the unsteadiness in the aerodynamics of these vehicles flying at low Re becomes tedious, and it is not efficiently predictable yet. An example of this, is given in the behaviour of the flow and the vortices produced on it, especially the leading edge vortex (LEV) that appears at the leading edge of the wings, in the case of MAVs, and that reattaches later on to the surface of the wing before trailing edge vortices (TEV) appears, (Sane 2003). Moreover, due to the small size of these vehicles, the task of including any navigation system, energy resources or efficient propulsive systems is still a trade off nowadays.

Thus, taking into account the difficulty concerning the study of the aerodynamics of this kind of motion, in the pages of this document, an analysis of the aerodynamic forces at low Reynolds number is presented. Due to the complexity of the real problem, the actual study is simplified in a two dimensional case (2D) assuming a wing of high aspect ratio and infinite spam. The motion analyzed is an oscillatory sinusoidal motion that combines pitching and heaving. Nevertheless, although the simplifications made are important, the immensity of the problem is still more than considerable, thus, if at the end of the document our knowledge about the aerodynamic forces and the performance that drives MAVs has increased, this project would worth it.

1.2 State of the art

To be able to analyze and recreate the exact motion of insects and small birds is a complex task for scientist, due to the small size and high frequencies in motion characteristics of these flying animals. Nevertheless, although the exact solution of the problem is difficult to be found, different approaches have been followed to achieve results that allow to simulate the flying movements of these animals, generating the necessary lift and thrust obtaining good results in terms of efficiency. In the past century with the development of aircraft and the increase on the aeronautical knowledge, different approaches have been followed to study the flapping motion at low Reynolds numbers. The construction of wind tunnels to recreate real life physics at a determine scale has supposed a way to analyze forces and moments by imposing different conditions in terms of the geometry of the immersed body, position of the body respect to an incoming velocity and different kinematics parameters that define the motion and that affects in a direct way to the aerodynamic forces and moments that are produced. These forces are measured by means of gauges, that allow to read the temporary response of forces and moments in computers. The experimental procedure of studying the flapping motion has been as important as the development of Computational Fluid Dynamics (CFD) simulations are, in which different procedures and numerical methods are applied to recreate real world physics where the temporary history of forces is not measured but computed. This two different but effective methods, of recreating and analyzing the movement of insects and small birds, have evolved with the past of the years, as well as the complexity of the simulations analyzed. Since the natural motion of these flyers is approximated to a flapping motion, defined as a combination between heaving and pitching motions, the research works have progressed from the study of these two motions separately, as a way of simplifying the problem, to the combination of both motions, which becomes a more complex task. Moreover, due to the huge amount of parameters that are involved in the problem, most of the studies have simplified the problem to a 2 dimensional one, where the flexibility and elasticity of the wing in the case of birds and membranes in the case of insects, have been suppressed. Despite all the studies made and the assumptions took, the complexity of understanding the flapping motion is startling for the scientific community.

Along the past century scientists have tried to understand and solve the problem of a 2D airfoil in heaving motion. Heaving motion was identify as the alternative to rotary propellers. When the vertical motion is produced the airfoil varies its angle of attack to a non-zero value, and the resultant normal force is decomposed producing thrust. This phenomena was explained, for the first time, in the research works of Knoller 1909 and Betz 1912 and it would be a decade later when Katzmayr 1922 validate these results thanks to an experimental study. Glauert 1930 and Garrick 1937 gave a lineal solution to the 2D problem that resulted to

be incompleted since it founds values of maximum propulsive efficiency at zero frequency. With the development in aeronautical knowledge and technology, the past of the years made that Jones and Platzer 1997 study the problem again. This time the non-linearities at the wake and the ones of the geometry of the airfoil were introduced in a model that used the unsteady panel method, but the frequencies obtained were not as good as expected. Moreover the generation of lift was also investigated. Carr 1988 set the concept of aerodynamic stall produced when the generation of lift is suddenly lost in steady aerodynamics. Later Ellington et al. 1996 studied the unsteady aerodynamics of the problem by means of Direct Numerical Simulations (DNS) and would state that the behaviour of the LEV and TEV were the main sources of lift generation in the airfoil. Moreover, Anderson et al. 1998, studied the relation between the thrust generated and the efficiency obtained with these vortical structures, LEV and TEV. With the beginning of the $21th$ century, Wang 2000 performed a numerical study of the problem, at a Re=1000, where it was established that an increase on the Strouhal number (St) produced and increase on the angle of attack, and thus, an increment on the generation of thrust. Moreover, it was observed how lift force increases at reduce frequencies, that increases the LEV and consequently its effect on lift. Independently, Young and Lai 2004 studied the strong dependence of the aerodynamic forces and wake structures on the values of reduced frequency and Strouhal number. Lewin and Haj-Hariri 2003 made a numerical study at Re=500 and states the dependency of propulsive efficiency on the LEV and TEV. Propulsive efficiency and thrust were penalized at low frequencies but at high frequencies propulsive efficiency also diminished similarly at what occurs assuming an inviscid theory. Thus, in terms of propulsive efficiency the optimum frequencies are obtained with the period of the shedding vortices. Moreover, it was stated that an increase in efficiency is produced increasing the separation time of the LEV and keeping it attached along a period of motion. A pattern on the vortical structures was also studied in order to analyzed the interaction between the LEV and the TEV. It was seen how with a reinforcement of the TEV with the LEV propulsive efficiency and thrust increases. Moreover, the increase on propulsive efficiency was higher when the shedding LEV was dissipating. Later on, Martín-Alcántara, Fernandez-Feria, and Sanmiguel-Rojas 2015 would develop a decomposition of the vortex forces to describe these interactions that take places on the wake structures. Moreover, it has to be mentioned the experimental studies of Lai and Platzer 1999, Lua et al. 2007 and Heathcote, Wang, and Gursul 2008.

Despite the improvements in the methods used to solve the problem along the years, lower values of thrust were obtained, this leads to change the way of research and scientist started to study the effect of pitching motion in thrust, in order to see the effects of the new kinematics parameters in the aerodynamic forces and wake structures. It was seen that a variation in the mean pitch angle affects directly to the generation of thrust and lift, and when non-zero values were

given to the pitching amplitude, the values obtained for propulsive efficiency and thrust improved. These parameters and a variation of the Reynolds number had a clear influence in the behaviour of the flow around the airfoil. Different experimental studies had been performed, between them it has to be recalled the one of Walker, Helin, and Chou 1985 whose study is based on the effects that pitching rate and Reynolds number has on the pressure field and the vortices generated around the airfoil. On the other hand the two independent experimental studies of Freymuth 1988 and Koochesfahani 1989 were focused on the explanation of the thrust generation in pure pitching motion. It was observed a relation between the frequency and pitching amplitude with the axial flow produced at the wake vorticities structures.

Furthermore, several studies that include these two motions can be found. The combination of pitching and heaving motion, increases the complexity of the problem due to the amount of parameters involved in it, that hamper the finding of the optimum combination of values for the kinematics parameters to allow values of maximum thrust, maximum propulsive efficiency and good results in terms of achieved lift. Theodorsen and Mutchler 1935 developed an inviscid, linear and unsteady theory to predict the forces generated. This theory would be used by Garrick 1937 to provide the expressions of the input and output power required by the airfoil and the mean thrust generated. McCroskey 1982 observed that before dynamic stall is produced large forces of short duration takes places. Triantafyllou, Triantafyllou, and Grosenbaugh 1993 announced that, for reduced frequencies and low values of feathering parameter, the observation of the wake structures overestimate the thrust generated. Moreover, as it was set for pure pitching motion, the LEV is one of the main sources of lift. For the case of flapping motion Ellington et al. 1996 explained that the spanwise flow component, derived by the pressure and velocity gradients that takes place by the acceleration at the boundary layer, is related with the way the LEV attaches to the surface of the airfoil and its stability, affecting in a direct way to the generation of lift. Anderson et al. 1998, was also interested in flapping motion and made several experimental studies varying parameters involved in the kinematics. He concluded that the generation of thrust was much higher when the shift angle between pitching and heaving motion was larger than 90^o. Dickinson, Lehmann, and Sane 1999 studied the nonsinusoidal movement in robots experimentally, where Magnus effect was appreciated, and Isogai, Shinmoto, and Watanabe 1999 how propulsive efficiency and thrust were influenced by dynamic stall. Ashraf, Young, and Lai 2011 made a numerical study where the effect of thickness, camber and Reynolds number on thrust were analyzed. Fenercioglu and Cetiner 2012 studied the flow patterns around the airfoil depending on the wake vortices structures. Later on Ford and Babinsky 2013 and Widmann and Tropea 2015 studied the flow around airfoils trying to explain the behaviour of the spanwise flow component that affects the stability of LEV as announced Ellington et al. 1996.

1.3 Objectives

With this project, it is pretended to know more about the unsteady aerodynamics that takes place flying at low Reynolds numbers. Along the project, different objectives are established, these objectives can be divided into short term goals and long term goals.

The long term goal and main goal of the project, is as said before, to better understand the unsteady aerodynamics of flapping flights at low Re. Concretely, this project is focused on achieving a range of values of feathering parameter (χ) at which the studied airfoil can operate reaching values of maximum propulsive efficiency and maximum generation of thrust. Moreover, the relation between the propulsive efficiency obtained and the lift generated, has to be analyzed looking for the optimum configuration between maximum propulsive efficiency, maximum generation of thrust and allowed lift. To make this possible, in the process, aerodynamic forces and moments have been analyzed as well as the flow vorticities around the airfoil.

To develop the study, short term goals are established and followed.

- To understand the tool use to execute the direct numerical simulations (DNS), is the first short term goal to be accomplished. This tool is a Two-Three dimensional Code of Unsteady Aerodynamics in Nature (TUCAN) built with more than six thousand lines of code, innumerable files and libraries. Although it is not pretended to understand everything of TUCAN, it is necessary to know how it works and its main characteristics.

- To perform a literature review once the problem to be studied is defined in order to increase the knowledge about the subject.

- To clearly define and calculate each one of the parameters involved in the kinematics of the airfoil, in order to ensure the desired values of lift coefficient for each one of the studied simulations.

- To be able to analyze the results obtained for each simulation in terms of kinematics parameters, aerodynamic forces and moments, propulsive efficiency and behaviour of the flow.

- To compare the results obtained with the ones of a companion project (Yuste 2017), being able to identify which are the main differences and why they are produced.

If at the end of this project, every single one of these short term goals is accomplished the successful of the long term goal will be ensure.

1.4 Contents

The structure of the present document can be decomposed into seven different chapters and an appendix. The information contained in each one of them is briefly explained in the following lines.

- Chapter 1 is divided into 4 subsections. First of all, a motivation to carry out this project is presented. After this, the state of art collecting part of the literature of other authors whose research projects are related with the actual one. The final goals of the current project are include in the objectives section, and a scheme of the distribution of the contents along the documents is presented in the actual section.

- Chapter 2 collects the information related with the methodology concerning the software and hardware. It includes the governing equations of the project, the most relevant aspects of the flow solver used and some characteristics of TUCAN.

- Chapter 3 is a summary of the presented problem of this project. In this chapter, the definition of the physical domain as well as the kinematics of the airfoil, the selection of the parameters and a description of the simulations can be find.

- Chapter 4 includes an analysis of the results obtained for the simulated cases. In the first part of the chapter an analysis of the forces and propulsive efficiency is developed. Then, the behaviour of the flow vorticity is included. To finish with a comparison between the results obtained in this project and those of a parallel project (Yuste 2017), that simplifies the model developed in (Moriche 2017) is presented.

- Chapter 5 presents a description of the socioeconomic impact, regulatory framework and a estimation of the necessary budget to accomplish this project.

- Chapter 6 includes a summary of the project, shows the main conclusions after the development of the whole project and provides some considerations for future related works.

- Appendix A presents an estimation of the budget needed to perform this project.

- Appendix B collects extra information about the development of a code to execute the simulations.

Chapter 2

Methodology

In this chapter it is developed the methodology followed to carry out the simulations in an in-house code that recreates Two(Three)-dimensional Unsteady Code for Aerodynamics in Nature. The chapter is composed by three sections. In the first one, the governing equations to solve the problem are set. The second one is related with the numerical methods followed, the definition of the computational domain and time marching, and how the body is included in this domain. The last one, includes a brief explanation of how TUCAN works.

2.1 Navier Stokes equations

The governing equations to recreate the behaviour of the flow around the airfoil, are the Navier Stokes equations. Mass conservation equation and the momentum conservation equation for an incompressible and 2D viscous flow are solved in the simulations.

$$\frac{\partial u_i}{\partial x_i} = 0 \tag{2.1a}$$

$$\frac{\partial u_i}{\partial t} + u_j \frac{\partial u_i}{\partial x_j} = -\frac{1}{\rho}\frac{\partial p}{\partial x_i} + \nu \frac{\partial^2 u_i}{\partial x_j \partial x_j} \tag{2.1b}$$

where, u_i is the fluid velocity, p is the pressure, ρ is the density of the fluid, ν the kinematic viscosity, t the time and x the distance.

Along the whole project, Reynolds number takes a remarkable importance while solving the Navier Stokes equations. Reynolds number is one of the most popular adimensional numbers in aerodynamics defined as $Re = \frac{\rho U_\infty L}{\mu}$, where ρ is the density of the fluid, U_∞ is the upstream velocity of the fluid, L is the characteristic length of the body submerged in the fluid and μ the dynamic viscosity. It allows us to predict at which point of the boundary layer, the flow starts its transition from laminar to turbulent. It depends on different parameters such as the geometry of the body, its roughness and the uniformity of the flow between others.

In the case of a pipe the boundary layer is laminar until a Reynolds number of 1000 is reached, and the transition to turbulent ends once Re reaches a value of 2000. On the other hand, assuming a flat plate this transition to a turbulent regime starts at a Re of $5{\cdot}10^5$.

The geometry of the body selected, to perform the numerical simulation study, is a NACA 0012 profile, that can be considered as something in between a pipe (because of the rounded curvature at the beginning of the body) and a flat plate. Concretely, the NACA 0012 profile is characterized for having a 12 % of maximum thickness and no camber, being this profile symmetric respect to the x-axes. Moreover, it is considered to be the profile of a wing of infinite span, so that the effect produced on the flow by the wing tip vortices can be neglected, and the problem can be solved as a 2D one.

For all these reasons, Re number is going to be taken as an important parameter in the whole project. Reynolds number can be estimated as the ratio between inertial and viscous forces $\left(Re \simeq \frac{inertial forces}{viscous forces}\right)$. Low Re number is considered, and thus, viscous forces can not be neglected, in fact, they will have an important role in the aerodynamics of the 2D simulations presented.

Since low Reynolds number is considered, an incompressible fluid predominates in the simulations. The advantage of having assumed incompressible flow is the absence of pressure waves propagation, that allows larger time steps and coarser grids in the simulation, reducing the computation time without penalizing the final result.

Moreover, to solve the Navier Stokes equations (equations 2.1), some boundary conditions and no-slip condition at the surface of the immerse body are imposed to the velocity of the flow to recreate real conditions.

- At domain boundaries: u_i=0 (no-slip)

- At body surfaces: u_i=Ui

where U_i is the velocity of the immerse body.

Furthermore, the force perceived on the submerged body by the fluid is given by:

$$\vec{F} = -\int_S p\vec{n}dS + \nu \int_S \vec{\omega} \times \vec{n}dS \tag{2.2}$$

where S is the surface of the body, p the pressure, n is the unitary normal vector pointing towards the fluid and ω the vorticity of the flow.

2.2 Flow solver

In order to solve the Navier Stokes equations previously mentioned different aspects have been implemented in TUCAN such as the appropriate numerical method to be used, the definition of the computational grid and boundary conditions and the presence of submerges body in the fluid. All these aspects are commented in detail the following subsections.

2.2.1 Numerical methods

Navier Stokes equations (equations 2.1) are solved in TUCAN thanks to a Direct Numerical Simulation (DNS) method that allows accurate results that are penalized by the computational costs of the method, since the flow solution of equations 2.1, is calculated at every single point of the mesh of the computational domain rather than the solution given by a theoretical method, which is cheaper but less precise.

On the one hand, a fractional step method is used to undertake the decoupling issue that presents the temporary independent continuity equation (equation 2.1a) as explained in Brown, Cortez, and Minion 2001, where the full algorithm of Runge Kutta k-th sub-step scheme is developed in detail. There it is explained how, the velocity components are obtained from the temporary dependent momentum equation (equation 2.1b). Moreover, this method applies a correction to the values obtained in order to fulfill and solve both Navier Stokes equations (continuity and momentum).

On the other hand to solve the spatial issue, a uniform staggered grid is discretized, and the spatial derivatives are approximated by the used of center finite differences with second order error convergence, and a three stage, low storage Runge Kutta scheme is applied to perform the time marching, where advective terms are treated explicitly and diffusion terms implicitly as it is described in Roma, Peskin, and Berger 1999, where the full method is explained with more detail.

2.2.2 Computational grid

Each simulation has its associated defined computational domain. The way to perform the spatial discretization in TUCAN is using uniform, structured and staggered grid. The domain is structured into cells, splited in x and z directions, in a uniform way, since the space between cells is the same in both directions and the fact of defining a staggered grid means that the points where the pressure and the normal components of the velocity are calculated is not the same (see figure 2.1).

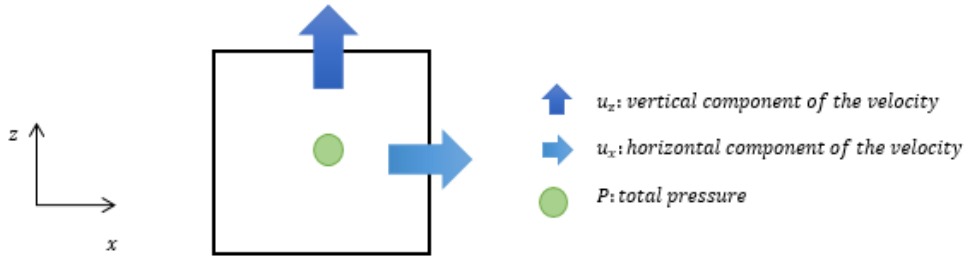

Figure 2.1: *Sketch of a cell of the staggered grid .*

The fact of using staggered grid instead of a collocated one, can be justify in different ways. While discretizing momentum equation (equation 2.1b) by second order finite differences, checker board oscillations used to appear in the case of a collocated grid. Nevertheless, these oscillations are suppressed using a staggered grid. Moreover, the need of calculating pressure and velocity components at different points, makes interesting the used of staggered grids where the spatial discretization becomes easier due to the relative position of grid points of the different variables.

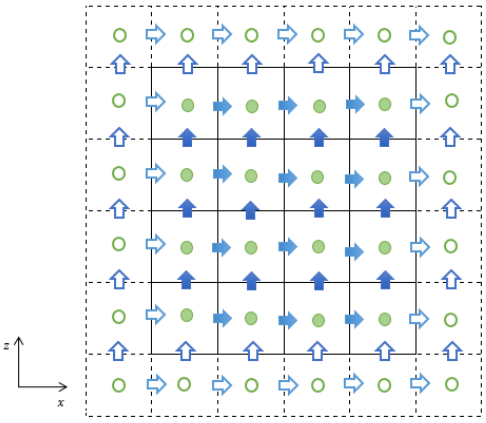

Figure 2.2: *Sketch of the grid .*

Figure 2.2 presents a sketch of the actual implementation of uniform, structured and staggered grids in TUCAN. As it is seen in the figure, the computational grid is subdivided uniformly and structurally in small regions building a mesh. At the centre of these regions (cells), total pressure is computed and at their boundaries the normal components of the velocity are calculated. The boundaries of the

computational grid domain lie on the nodes of the normal components of the velocity.

This kind of grid is applicable in TUCAN to simulations whose boundaries conditions are characterize by free slip boundary conditions at the north and south of the computational grid, inflow and outflow boundary conditions are set to the east and west regions and Neumann boundary conditions are applied to the pseudo-pressure.

Moreover, it has to be commented the presence of ghost points on the computational grid which are represented on figure 2.2 by empty symbols. These ghost points are a very important and relevant aspect that has to be taken into account in the implementation in TUCAN, since at these points of the grid the solution cannot be calculated in TUCAN. Instead, they are used in the computations during the execution process or as initial condition of an existing field. In section 2.3.1 it is explained how the solution of these ghost points is obtained.

2.2.3 Boundary conditions (BC)

To recreate real world physics TUCAN tool is provided with different boundary conditions (BC):

- Advective condition: is applied at those boundaries of the domain where possible reflections of the flow while it is leaving the computational domain want to be avoided, so that the actual solution compute inside the domain is not affected but this exiting flow.
- Dirichlet condition: consists on specifying the value of the solution.
- Neumann condition: imposes the value of the derivative.
- Periodic condition: whenever a variable of the flow has a periodic repeated pattern in time. The advantage of this BC is that once a period is completed the behaviour can be known in advance.

Having defined the possible boundary conditions, Dirichlet, Neumann, advective and periodic boundary conditions can be set at any of the boundaries of the computational domain. Nevertheless, it has to be recall the benefits of using advective boundary conditions at the east boundary of the domain. As it is seen in the definition of this type of boundary condition, in the presence of intense flow at the outlet of the domain an advective process is produced. By using this type of boundary condition reflections at the outlet of the boundary, that can be produced by using Neumann or Dirichlet boundary conditions, are avoided, helping that the flow structures can leave the computational domain as smooth and in the more realistic way as possible. Thus, the equation to compute the

actual solution at the east boundary using advective boundary conditions is the following one.

$$\frac{\partial \vec{u}}{\partial t} + C\frac{\partial \vec{u}}{\partial x} = 0 \tag{2.3}$$

where C is the advective velocity, assumed to be constant in that boundary in order to fulfill mass conservation inside the computational domain (Ferziger and Peric 2012). This equation (equation 2.3), is solved following the Runge Kutta k-th sub step scheme for an advective boundary conditions, similarly as it is done with the momentum equation (equation 2.1b) (Brown, Cortez, and Minion 2001).

On the other hand, the use of periodic boundary conditions affects the definition of the staggered grid, whose grid points are going to differ from those of the grid used while Neuman or Dirichlet boundary conditions are applied. Figure 2.2 shows the effect of using periodic boundary conditions in x and z directions on the computational grid points distribution.

Finally, since incompressible flow is assumed, the boundary condition chosen for the pressure in the whole computational domain is Neumann condition.

2.2.4 Immersed Boundary Method (IBM)

In order to solve NS equations in the presence of a submerged body, the Immersed Boundary Method (IBM) is considered. This method provides high computational efficiency, specially in the presence of moving rigid bodies at low Reynolds numbers. If higher Reynolds numbers were considered, this method should be fitted in order to provide higher resolution accordingly to the boundary layer that will be thinner.

Although the cost associated with the definition of the grid is considerable, it compensates the costs derived while using a body-fitted method, that has to remesh the grid and do interpolations continuously to solve the algorithm of the problem. The use of IBM in TUCAN, simplifies and facilitates the discretization of the computational grid for complex body geometries, and in the presence of moving bodies the tasks required of remeshing and interpolating needed in body-fitted methods are suppressed due to the computational saving resources that IBM presents. (Mittal and Iaccarino 2005)

To take into account the presence of the body inside the fluid two different domains are defined: the Eulerian one which is fixed (fluid), and the Lagrangian which is the moving one (body). A regularized delta function, which is a discrete version of the Dirac´s delta function introduced by (Peskin 2002), with a three points stencil is used in a diffuse discrete forcing approach method that interpolates from the Eulerian to the Lagrangian mesh. The body immersed in the

fluid is considered to be rigid, the kinematics of the body movement are known and imposed, and the interaction between it and the fluid is unidirectional. The presence of the body in the fluid is allowed by adding a force term in the right hand side of the momentum equation (equation 2.1b) to ensure the no-slip condition and fix the velocity at the boundaries of the body. In Uhlmann 2005, it is described with more detail the IBM implemented in TUCAN.

Thus, considering the presence of a rigid moving body inside the fluid, the algorithm to solve the Navier Stokes equations inside the computational domain follows the next steps:

1. An explicit estimation of the velocity in the Eulerian mesh is done.
2. Using the regularized delta function previously mentioned, an interpolation between the velocity in the Eulerian to the Lagrangian frame is performed.
3. The volume force from the estimated Lagrangian velocity and the desired one is computed in order to preserve the no-slip condition at the Lagrangian points.
4. This volume force is transform from Lagrangian to Eulerian frame.
5. Introducing the volume force term into the Navier Stokes momentum equation (to the right hand side), they can be solved following the fractional Runge Kutta k-th sub-step method.

An important fact that has to be commented is that with the movement of the Lagrangian frame, the same does the node points associated to it, where the components of the velocity and the pressure are calculated. This point that at the beginning where points of the body without historical data, become into fluid points with the movement of the frame producing some fluctuations in the calculated results. These fluctuations are corrected thanks to the used of a low pass filter that introduces in that points without historical data, the calculated average of the points in the surroundings.

2.3 TUCAN

The numerical simulations are carried out using TUCAN (Two or Three Dimensional unsteady Code for Aerodynamics in Nature), which is an inhouse code of significant complexity. It has around 60 thousand lines of code, uses external libraries and requires specific machine configurations to work properly. This tool, is already validated for different canonical 2D laminar cases such as Taylor Green vortices, Poiseuille flow, stationary and moving cylinders and airfoils; and 3D cases such as flow around a sphere and fully-developed turbulent channel flow

inside a channel (Moriche 2016). Thus, TUCAN has been already implemented and it is in continuous used in other investigation works to recreate real world physics.

In the following subsections, a brief description of the parallelization as a way of processing and solve the required linear systems of the numerical simulations and how TUCAN works with Input/Output tasks, is included (Moriche 2017).

2.3.1 Parallelization

The simulations in TUCAN are executed by a parallelization process that is based on Messege Parsing Interface (MPI) standard (Forum 1994). The main characteristic of MPI standards, is that during a run, processes do not share memory, in fact, if they need information of another process they have to communicate between them, which is a complex task. Nevertheless, MPI standards present some advantages that shared memory protocols, as it is the case of Open MP (Dagum and Menon 1998), do not present. MPI standards allow the possibility of increasing the number of processes in a run in a "indefinitely" way. On the other hand, share memory protocols only can use the number of processors in a run up to the number of processors that are allowed in the machine, and increasing this number implies a notorious cost.

Every single simulation performed in TUCAN has its corresponding defined physical domain, where Navier Stokes equations have to be solved to get the aerodynamics of each problem. The way to distribute the workload is by following a partition strategy in which the domain, and the corresponding grid assigned to it, are decomposed in different portions distributed uniformly in x and z directions, and said portions are assigned to different processes. Despite the distribution of the domain in these regions, there are other overlapping regions assigned to different processes that help to cover the ghost points of the mesh (see figure 2.2). At this point of the computational process, a communication between the information of processes is required to cover the missing information of ghost points. This communication is performed twice in each step (for each of the computational variables, which are the velocity components and the pseudopressure), once the solution of the linear system is calculated and once the correction of the solution is performed.

2.3.2 Linear systems

To obtain the aerodynamics inside the defined domain of the studied problem, NS equations (equation 2.1) are solved thanks to the implementation in TUCAN of the numerical method previously described in section 2.2.1, where the solution of a linear system for each component of the velocity is obtained solving the Helmholtz

problem in an iterative process (the matrices present a dominant diagonal) and the solution of the linear system for the pseudopressure is given solving the Poisson problem where finite differences are needed to define the spatial discretization of the problem (matrices are sparse). For this reason, Poisson problem uses Hypre routines ("High performance preconditioners" 2016 June) that has been shown to work more than efficiently enough in massive parallel computers (Baker et al. 2012). Moreover, to solve this problem a solver based on multigrid method has to be preconditioned, which is an expensive but effective method. On the other hand, to solved Helmholtz problem, a conjugate gradient solver is required.

2.3.3 Input/Output tasks

As it is mentioned above, TUCAN is fully composed of libraries and routines. During the execution of the code to perform a desired simulation lots of Inputs/Output tasks (I/O) take place in order to write/read existing data to/from a file with the purpose of storing data, reading this existing data or postprocessing it. Regarding with this Input and Output tasks, it has to be mentioned that the time needed to access to data increases exponentially when the number of processor that requires access to this data increases, so there should be a balance between the performance of the simulation and the information desired to be storage by the user. Moreover, the time needed to access to a disk is higher than the time of accessing memory.

For these reasons, the Hierarquical Data Format version 5 (HDF5) libraries are used in TUCAN as the best option of storage, providing I/O routines while handling MPI standards (Group 2016). Thus, HDF5 protocol allows the storage of large buffers of data in a unique output form that results of easy access and are easily read by postprocessing data tools, like Matlab, that includes libraries and routines to read and write data in this format version.

Chapter 3

Problem

In the sections and subsections of this chapter, relevant aspect concerning the simulations of this project are contained. The chapter has been divided into two sections. The first one contains information about how the problem has been defined in TUCAN. In the second one, the physics of the problem and how it has been carried out is explained.

3.1 Computation and set up

In this section the definition of the computational domain, body geometry and boundary conditions of the project in TUCAN are explained.

3.1.1 Computational domain

All the simulations performed along the project are carried out in TUCAN, where Navier Stokes equations are solved in a box of dimensions $12c$ in x-direction and $10c$ in z-direction. The term c refers to the chord of the airfoil, taken as the characteristic unit of length. Said box, defines the computational domain that has its associated computational grid characterized to be uniform, structured and staggered, as it was explained in section 2.2.2.

Looking at figure 3.1, it can be seen how the airfoil is placed at the origin of axis at mid high of the computational box. Nevertheless, the $12c$ in x direction has been distributed leaving $3c$ upstream and $9c$ downstream where the aerodynamics at the wake structure are more complex.

The computational grid is subdivided into cells that configure a mesh. Since the resolution selected is of 64 points per chord, the grid is composed by a total number of 491,520 grid points, being N_x=768 the number of grid points in x-direction and N_z=640 the number of grid points in z-direction. To ensure the uniformity of the grid, the mesh width is defined to be the same in both directions (x and z) in such a way that $\Delta x = \Delta z$. The mesh width is computed as follows:

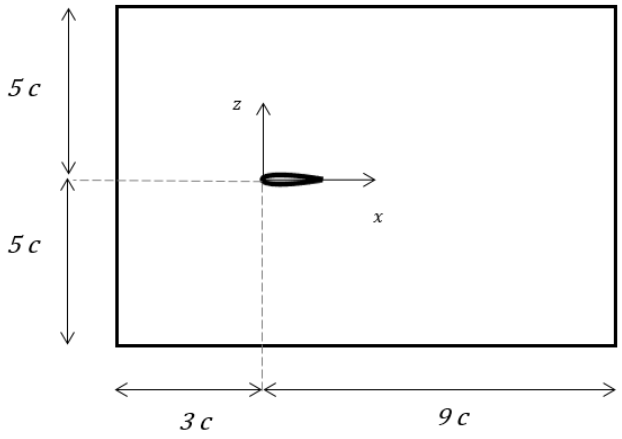

Figure 3.1: *Computational domain.*

$$\Delta x = \frac{x_f - x_0}{N_x} \tag{3.1a}$$

$$\Delta z = \frac{z_f - z_0}{N_z} \tag{3.1b}$$

where x_0 and x_f represent the initial and final coordinates of the computational domain in x-direction and z_0, and z_f are the initial and final coordinates respectively in z-direction, so that $\Delta x = \Delta z = \frac{1}{64}$

It has to be commented that the dimensions of the domain and the resolution of the computational grid are adapted for a problem of Re=500. If this number was increased, the resolution should be increase as well, since the thickness of the boundary layer will decrease and the resolution has to be adjusted to the requirements and necessities of the problem to obtain accurate results.

3.1.2 Definition of the submerged body

In section 2.1, it was briefly commented that the submerged body selected to be inside the fluid domain is a NACA 0012 profile, with no camber and maximum thickness of 12% of its chord.

As it is done with the computational grid, the submerged body is also defined and discretized. A uniform distribution of points along the surface of the airfoil is perform taking into account that the resolution is of 64 points per chord, so that the total number of points needed to build the surface of the airfoil is of 131 points. The discretization in TUCAN is performed following the scheme described

by Uhlmann 2005, where in appendix A.1, the procedure is fully developed in detail for the case of a circumference. During the discretization, the requirement of having the differential of volume associated to each Lagrangian point as close as possible to the square of the cell width is kept ($\Delta V \simeq \Delta x^2$). With a resolution of 64 points per chord the associated volume obtained is $\Delta V/c^2 = 2.433 \cdot 10^{-4}$ while $\Delta x^2 = 2.441 \cdot 10^{-4}$ having an error of the 0.32%. Doing the transformation from the Lagrangian to the Eulerian frame, as explained in section 2.2.4, and once the airfoil is defined with this configuration, 64 grid points are needed in x-direction and 7 grid points at the maximum thickness section of the airfoil.

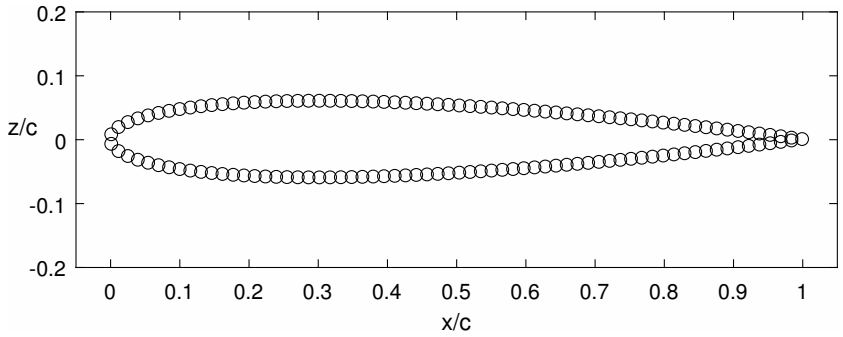

Figure 3.2: *Lagrangian markers for a NACA 0012 profile with a resolution of 64 points per chord.*

3.1.3 Boundary conditions

Having defined all the possible types of boundary conditions that can be applied in TUCAN (see section 2.2.3), the boundary conditions applied to all the direct numerical simulations (DNS) of the present project are presented.

As it is seen in previous section (section 3.1.1), the submerged body, a NACA 0012 is placed at the origin of the computational domain. Three chords upstream of the leading edge (LE) of the mentioned NACA, a uniform free stream, of velocity U_∞ in the x-direction, is imposed just at the inlet boundary of the domain where Dirichlet BC are applied to both components of the velocity (x and y components) and at the exit of the domain, nine chord upstream, advective BC are applied to avoid the possible reflections commented previously in section 2.2.3. Finally, on both vertical boundaries, free-slip boundary conditions are applied so that there is no penetration of fluid either entering or exiting of the domain. This is achieved imposing Neumann BC at the x component of the velocity and Dirichlet BC at the y component. Finally Neumann boundary condition is applied to pressure in the whole domain.

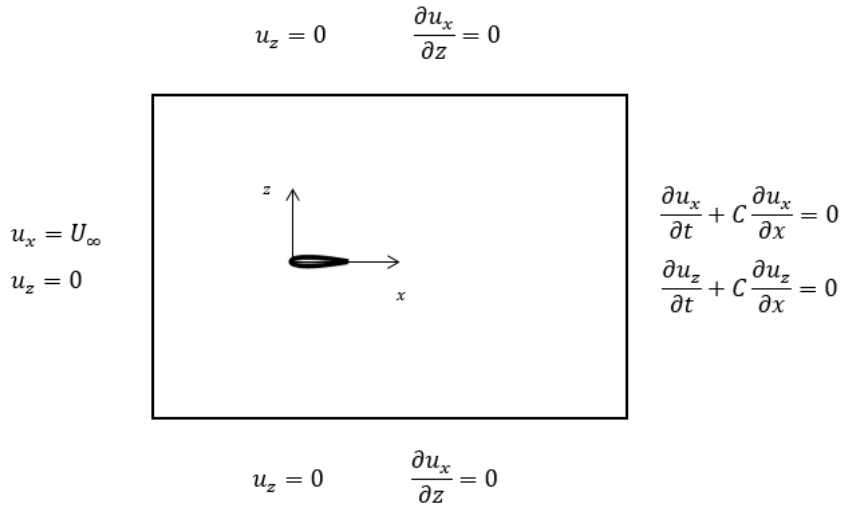

Figure 3.3: *Applied boundary conditions at the computational domain .*

3.2 Physics of the problem

These sections include information regarding the kinematics of the problem, the definition of the parameters involved in it and all the steps followed to carry out the simulations.

3.2.1 Airfoil motion

All the simulations are performed at a Reynolds number of 500 which is defined as:

$$Re = \frac{\rho U_\infty c}{\mu} \tag{3.2}$$

where the free stream velocity (U_∞), the characteristic length which is the chord of the airfoil (c), the density of the fluid (ρ) and the dynamic viscosity of the fluid (μ) are involved.

The kinematics of all the Direct Numerical Simulations of this project, are carried out in TUCAN. Figure 3.4 shows and sketch of the main kinematics features and the parameters involved in the motion of the airfoil.

In figure 3.4, it is seen how many parameters are involved in the kinematics of the airfoil. Those parameters are the distance from the LE to the pivoting point,

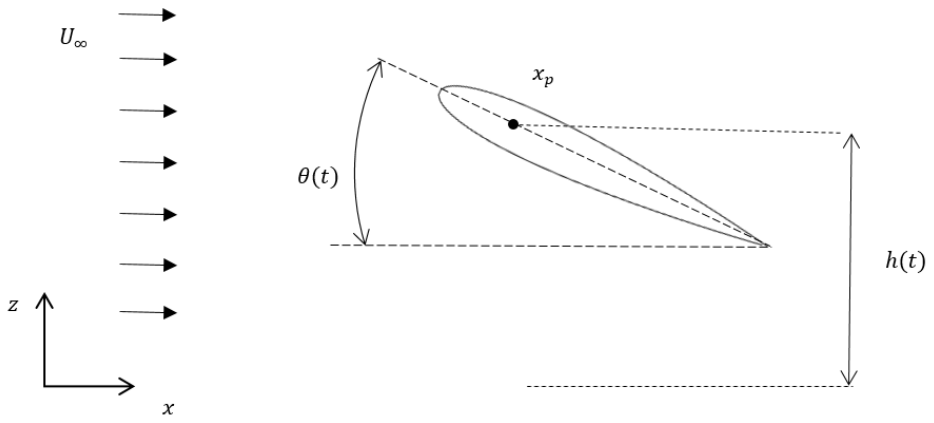

Figure 3.4: *Sketch of the kinematics parameters involved in the motion of the airfoil.*

defined to be as one quarter chord ($x_p = c/4$), the pitching amplitude (θ_0), the mean pitch angle (θ_m) and the heaving amplitude (h_0), all of them affecting in a direct way to the equations of motion that are given by:

$$h(t) = h_0 \cos(2\pi f t) \tag{3.3a}$$

$$\theta(t) = \theta_m + \theta_0 \cos(2\pi f t + \varphi) \tag{3.3b}$$

Equation 3.3a defines the heaving motion of the airfoil in time, being $h(t)$ the vertical displacement of the pivoting point, while equation 3.3b defines the pitching motion in time, where $\theta(t)$ is the pitching angle, defined to be the angle between the chord line and the free stream velocity direction. In equations 3.3, it can be seen how both movements are carried at the same frequency of motion (f), but with a phase shift difference between the heaving and pitching motions (φ). The frequency of the motion can also be defined by means of the reduced frequency k.

$$k = \frac{2\pi f c}{U_\infty} \tag{3.4}$$

It has also been taken into account the periodicity of the movement of the airfoil. This periodicity is defined by the period of oscillation which is the inverse of the frequency of the motion (f), so that:

$$T = \frac{1}{f} = \frac{2\pi c}{k U_\infty} \tag{3.5}$$

Along the computational process, the aerodynamic forces and moments are computed several times in each period. The way to perform the temporary discretization is by defining the time step and thus, the number of steps per period. Both parameters are influenced by the Courant Fredrich Levy (CFL) condition which indicates until which point the computational process is stable and can converge to a solution. The formula to calculate the non-dimensional CFL number is given by:

$$CFL_{max} > CFL_{simulation} = \frac{U_{max}\Delta t}{\Delta x} \tag{3.6}$$

where CFL_{max} is the maximum CFL that the simulation allows in terms of stability, $CFL_{simulation}$ is the maximum calculated CFL of the simulation, U_{max} is approximated to be twice the income free stream velocity (U_∞), Δt represents the time step and Δx the mesh width defined previously in section 3.1.1. Isolating Δt in equation 3.6 and knowing that the number of steps per period is defined as:

$$n_{steps} = \frac{T}{\Delta t} \tag{3.7}$$

A first approximation of the number of steps per period is done. Nevertheless, this number is rounded to the nearest possible power of two, since this will facilitate the postprocessing of data. Thus, the new value for the time step parameter is introduced in equation 3.6 to check the stability of the simulations.

Being periodic all the presented simulations in this project, their motion can schematically be presented as follows:

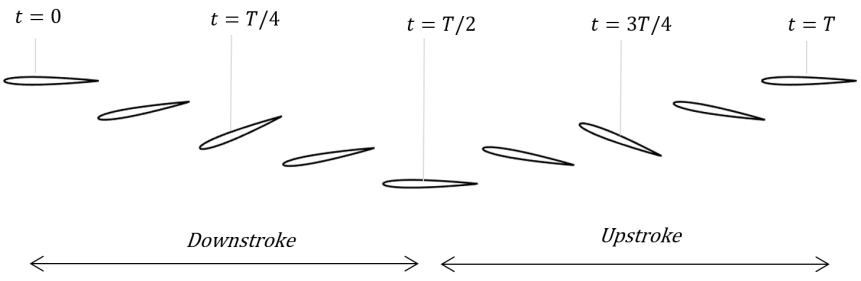

Figure 3.5: *Sketch of the airfoil motion along a period.*

where it has to be remarked the distinction between the downstroke motion at the first middle of the period, and the upstroke motion in the second part of the period.

3.2.2 Selection of the parameters

Due to the big number of parameters that affect to the kinematics of the airfoil, the fact of study their effects on the motion and the aerodynamic forces is unmanageable. Thus, some parameters have been selected to be fixed along the whole project while others have been varied for each simulation.

The parameters that have been fixed and their respective values are:

- Number of resolution points per chord. $p.c = 64$
- Reynolds number. $Re = 500$
- Heaving amplitude. $h_0 = c$
- Pivoting pint. $x_p = c/4$
- Reduced frequency. $k = 1.41$
- Oscillation period. $T = 4.44c/U_\infty$
- Time step. $\Delta t = 2.16 \cdot 10^{-3}$
- Number of steps per period. $n_{steps} = 2048$
- Phase shift. $\varphi = 90^o$

On the other hand, there are several parameters that have been varied in every simulation, some of them have been imposed and there are other parameters that are dependent of the previous ones. The independent parameters are the mean lift coefficient($\bar{c_l}$) and the feathering parameter (χ) while the mean pitch angle (θ_m) and the pitching amplitude (θ_0) are the dependent ones, and its calculation will be explained in next section (section 3.2.3).

First of all, the DNS are executed imposing different values of mean lift coefficient ($\bar{c_l}$). The selected values are : 0, 0.25, 0.5, 0.75, 1 and 1.5.

The feathering parameter has been one of the most relevant parameters of this project. It is defined as:

$$\chi = \frac{\theta_0}{\arctan\left(\frac{\omega h_0}{U_\infty}\right)} \tag{3.8}$$

where ω defines the angular velocity given by:

$$\omega = 2\pi f = \frac{kU_\infty}{c} \tag{3.9}$$

For very low angles, it can be approximated to $\chi = \frac{\theta_0 U_\infty}{\omega h_0}$ (something as the ratio between the movement of pitching and heaving described by the airfoil), but in the studied cases this assumption can not be made. If $\chi = 0$ pure heaving motion is presented, values of $\chi < 1$ indicate propulsive cases, values of $\chi > 1$ describe power extraction cases and for values of $\chi = 1$ a neutral motion (feathering) is presented where the airfoil movement is smooth with the flow. The selected values of feathering parameter for this project are in the range from 0 to 1. At the beginning, it was decided to start from 0 increasing the value 0.2 each time until 1 in order to have a global vision of how this parameter affects to the kinematics. Later, it was seen that a feathering parameter of 0.5 and 0.7 were points of interest in terms of maximum thrust and maximum propulsive efficiency respectively. So that at the end, the studied values of χ are: 0, 0.2, 0.4, 0.5, 0.6, 0.7, 0.8 and 1.

Taking this into account, and looking at the definition of χ (equation 3.10), the dependence of the pitching angle (θ_0) to the feathering parameter is clear. Isolating θ_0 from this equation, this parameter can be calculated for each simulation as:

$$\theta_0 = \chi \cdot \arctan\left(\frac{\omega h_0}{U_\infty}\right) \tag{3.10}$$

Every selected value of feathering parameter has its corresponding value of pitching amplitude in the simulation. These values, are collected in table 3.1.

χ	0	0.2	0.4	0.5	0.6	0.7	0.8	1
θ_0 (^{o})	0	10.94	21.89	27.36	32.83	38.30	43.78	54.72

Table 3.1: *Corresponding values of pitching amplitude angle for each feathering parameter.*

3.2.3 Description of the simulations

As it is specified in section 3.2.2, six different values of lift coefficient and eight different values of feathering parameter are studied. In this project all the possible

combination between them are executed, performed and analyzed yielding in a total number of 48 simulations. Since the amount of data regarding these simulations is huge, the most relevant results will be presented on chapter 4 following table 3.2.

χ \ $\bar{c}_l$	**0**	**0.25**	**0.5**	**0.75**	**1**	**1.5**
0	C00000	C00025	C00050	C00075	C00100	C00150
0.2	C02000	C02025	C02050	C02075	C02100	C02150
0.4	C04000	C04025	C04050	C04075	C04100	C04150
0.5	C05000	C05025	C05050	C05075	C05100	C05150
0.6	C06000	C06025	C06050	C06075	C06100	C06150
0.7	C07000	C07025	C07050	C07075	C07100	C07150
0.8	C08000	C08025	C08050	C08075	C08100	C08150
1	C10000	C10025	C10050	C10075	C10100	C10150

Table 3.2: *Summary of the simulated cases in TUCAN.*

Table 3.2 collects the names of all the simulations performed in TUCAN. The scheme to name the cases is easy to follow. As it is seen all the names are composed by a C followed by 5 digits (CXXYYY). Letter C refers to the studied "Case", the next two digits (XX) account for the selected value of feathering parameter for the simulation, and the last three digits (YYY) refer to the target value of mean lift coefficient.

The aim of performing all these simulations, is to find at which feathering parameter, maximum thrust and maximum propulsive efficiency are reached for each one of the different desired values of mean lift coefficient. The simulations are performed following an iterative process in which some of the parameters involved in the equations of motion are fixed, others vary and some of them are estimated as a first approach to reach said $\bar{c}_{l_{target}}$.

All the tasks, concerning the simulations, performed in this project can be classified in: preprocessing tasks, processing tasks, postprocessing tasks and analysis tasks.

Before launching any simulation in TUCAN, the computational domain, boundary conditions and body geometry need to be specified. This, and the parameters involved in the equations of motion are included in the required libraries and files. As explained in section 3.2.2, while solving the time history of the equations of motion, h_0, k, φ and x_p are kept fixed for all the performed simulations, θ_0 varies according to the value of χ and θ_m is firstly estimated and then adjust, as will be explained in the following paragraphs, to achieve the desired $\bar{c}_{l_{target}}$.

The project is started for cases whose $\bar{c}_{l_{target}} = 0.5$. The estimation of θ_m is done looking for a similar simulation case in Moriche 2017. There, the case B090 is selected. The characteristic parameters of this case are: $\theta_0 = 30^o$, $\theta_m = 10^o$, $\varphi = 90^o$, $x_p = c/4$, $h_0 = c$ and the $\bar{c}_l$ obtained with them is of 1.5509. The most similar value to that θ_0 in this project, is the one provided for $\chi = 0.6$ ($\theta_0 = 32.83^o \simeq 30^o$). Thus, the first studied case for $\bar{c}_{l_{target}} = 0.5$ is the case C06050. By means of a linear interpolation using this data, and taking into account that θ_0, φ, x_p and h_0 are the same in both cases, a value of $\theta_m = 3.33^o$ is obtained as a first approximation to reach a $\bar{c}_l = 0.5$ which is considered a good approximation, since the final value calculated of θ_m to reach said $\bar{c}_l$ is of 3.81^o. With this case converged, the same procedure is used to estimate an initial value of θ_m, in all the studied cases, that are introduced in the appropriate file in TUCAN.

Once the preprocessing tasks are performed, TUCAN is in charge of the execution of the DNS. At this point of the simulation, the Navier Stokes equations (equations 2.1) and the equations of motion 3.3 are solved processing the provided data and parameters. Once the launched simulation is converged[1], TUCAN provides different output data that has to be analyzed doing some postprocessing tasks.

The historical data of the normal components of the velocity and forces, momentum, pressure, values for the vertical displacement and pitching angle between others, are provided by TUCAN. In order to ensure that the simulation has converged to the desired lift coefficient, a code to facilitate the postprocessing of data has been developed, although it has not been automatized in TUCAN, since the complexity of doing this, does not compensate due to the fastness of the simulations to converge[2]. A summary of the main tasks of this code is developed in the following lines.

- First of all, it is check whether the simulation is converged or not. This is done by analyzing the forces obtained for the launched simulation. Assuming that at least two periods of the simulation are calculated in TUCAN. The average of the lift coefficient of one period is compared with the one of the previous period until the absolute difference between them is lower than an arbitrary tolerance defined to be $1 \cdot 10^{-4}$.

$$|\bar{c}_l(i) - \bar{c}_l(i-1)| < 1 \cdot 10^{-4} \tag{3.11}$$

  where i represents the number of the period starting from 2.

[1] Each launched simulation in TUCAN, takes around 7 hours and 15 periods of simulation to converge with the input parameters provided, and needs 2-3 iterations of θ_m to converged to a desired value of $\bar{c}_{l_{target}}$.

[2] It was expected that at least 5 iterations were needed for each simulation to converge.

- If this condition is not satisfied, the simulation has to be relaunched until it converges, otherwise the step to follow is to check if the simulation has achieved the desired $\bar{c}_{ltarget}$. This is done calculating the error between the average lift coefficient achieved in the last period of the simulation, and the desired mean lift coefficient. Again, an arbitrary tolerance of 0.2% is used in the checking process.

$$\left| \frac{\bar{c}_{ltarget} - \bar{c}_l(i)}{A} \right| < 0.2\% \tag{3.12}$$

  where A represents the amplitude of signal of c_l for the last calculated period of the historical data. If the error is lower than the defined tolerance, the simulation is converged to the desired solution and the historical data for the last period, once it has converged, is stored to be analyzed later on.

- If the simulation is not conclude, a new value of θ_m is calculated to reach the desired $\bar{c}_{ltarget}$. This is done by means of the secant method, knowing for the first iteration that for $\theta_m = 0$, $\bar{c}_l = 0$, and once the second iteration is performed, using the values of θ_m and $\bar{c}_l$ achieved in the previous iteration.

$$\theta_{m_{root}} = \theta_{m_{current}} - \frac{\left(\bar{c}_{lcurrent} - \bar{c}_{ltarget}\right)\left(\theta_{m_{current}} - \theta_{m_{old}}\right)}{\bar{c}_{lcurrent} - \bar{c}_{lold}} \tag{3.13}$$

  There $\theta_{m_{root}}$ is the new calculate value for θ_m, the variables with the subindex *current* refers to the ones of the last period of the actual simulation, and the variables with the subindex *old* define by the parameters of the previous iteration.

  At this point a new checking is performed in order to ensure that the solution given by the secant method has not diverged. The absolute difference between the current and new θ_m has to be lower than a new tolerance of 0.1^o.

$$|\theta_{m_{root}} - \theta_{m_{current}}| < 0.1^o \tag{3.14}$$

- Once the new calculated value of θ_m is computed the simulation is launched and the explained procedure is followed once again until the simulation is conclude.

For more details a flowchart and a pseudocode of the actual code implemented in the project are included in appendix B.

Last, but not least, some analysis tasks are performed. These tasks can be decomposed in the analysis of forces, visualization of the flow and a comparison between the results obtained in the actual project and a parallel project (Yuste 2017).

In the first part of the analysis, forces are analyzed paying special attention to the behaviour of thrust coefficient and propulsive efficiency. The motion of the airfoil is analyzed in terms of the non-dimensional lift and thrust coefficient.

$$c_l(t) = \frac{2F_z(t)}{\rho U_\infty^2 c} \tag{3.15a}$$

$$c_t(t) = -\frac{2F_x(t)}{\rho U_\infty^2 c} \tag{3.15b}$$

where F_x and F_z represent the streamwise and vertical components of the force respectively. Nevertheless, it has to be mentioned that since the project is studied in a non-dimensional way, such that the results can be adapted to any dimensions, in TUCAN forces are given in a non-dimensional way so that $F_{y_{TUCAN}}(t) = \frac{F_y(t)}{\rho U_\infty^2 c}$ and $F_{x_{TUCAN}}(t) = \frac{F_x(t)}{\rho U_\infty^2 c}$. Moreover, it has to be taken into account that TUCAN calculates the force exerted by the body on the fluid, and from an aerodynamic point of view, the force exerted by the fluid on the body is more interesting to be analized. Thus, when analyzing the forces provided by each simulation, it has to be considered, that for this project, the actual lift and thrust coefficients are given by:

$$c_l(t) = -2F_{y_{TUCAN}}(t) \tag{3.16a}$$

$$c_t(t) = 2F_{x_{TUCAN}}(t) \tag{3.16b}$$

Propulsive efficiency is also analyzed in this project. It is defined as the ratio between the ability of the airfoil to generate thrust and the work required to produce the periodic motion of the airfoil (combination of pitching and heaving motion). Its calculation for each simulated case is performed as follows:

$$\eta_p = \frac{T\bar{F}_x U_\infty}{\int_0^T (F_z\dot{h} + M_{y,c/4}\dot{\theta})dt} \tag{3.17}$$

where $M_{y,c/4}$ is the aerodynamic moment about the pivoting point located at the quarter of the chord of the airfoil, $\dot{h}$ and $\dot{\theta}$ represent the first time derivatives

of the heaving and pitching motion, previously defined in equations 3.3. The equations that define these two variables are:

$$\dot{h}(t) = -2\pi f h_0 \sin(2\pi f t) \tag{3.18a}$$

$$\dot{\theta}(t) = -2\pi f \theta_0 \sin(2\pi f t + \psi) \tag{3.18b}$$

Once the analysis of the forces is conclude a visualization of the vorticiy of the flow is performed, in order to relate the results obtained with the effect that some vortical structures, as it is the case of the LEV and the TEV, have on them.

This last tasks about the analysis of the data obtained for each simulation has been done using Matlab, a computational software. The most interesting results obtained will be developed in detail in next chapter (chapter 4).

Chapter 4

Results

This chapter collects the most interesting results obtained after the execution of this project. The chapter is divided into three sections. The first one is focused on the aerodynamic forces obtained in the simulations. The second one presents a visualization of the flow along a period of simulation, for the most relevant cases, in order to see how the LEV and TEV affect to the aerodynamic forces. The last section shows a comparison between the aerodynamic forces obtained in this project and the ones of a parallel project (Yuste 2017), in order to check the validity of the method applied in the last one.

4.1 Aerodynamic forces

The simulations are carried out according to the steps described in section 3.2.3. Due to the high number of studied cases the most relevant results obtained in each one of the simulations are collected in tables following the scheme presented in table 3.2.

Before analyzing the forces obtained, once the simulations have converged, the mean lift coefficient values are analyzed. The efficiency of TUCAN and the method used in the process, surprise due to the good results obtained in less than a day of computations per each launched simulation.

Figure 4.1 shows the mean lift coefficient values as a function of the feathering parameter for each one of the 48 simulated cases and the exact values obtained are collected in table 4.1. Looking at said table, it can be appreciated how the obtained mean lift coefficients are very similar to the target ones. As specified in section 3.2.3 the error between the obtained and target values is calculated (see equation 3.12) to ensure the convergence of all the simulations following the same criteria. It is established that the calculated error for each simulated case should be lower than a 0.2%. The results obtained are included in table 4.2. It is seen how the errors obtained are in almost all the cases an order of magnitude or even two orders of magnitude lower than the criteria established, being the highest error obtained of 0.17 % for the case C10075. With these results for the

calculated errors, the accuracy of the results obtained in terms of aerodynamic forces and other parameters is more than ensure for the presented problem.

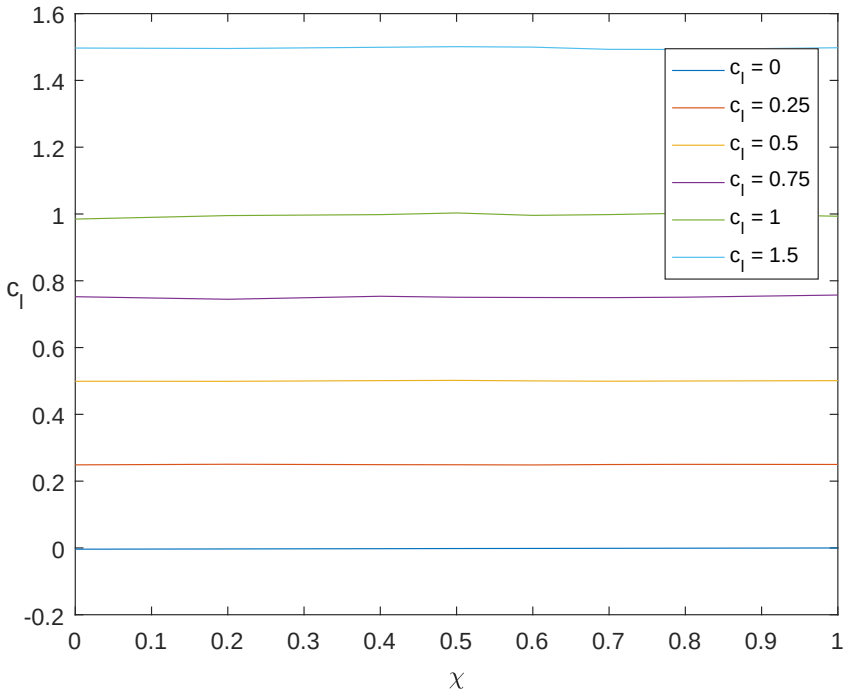

Figure 4.1: *Mean lift coefficient ($\bar{c}_l$) as a function of feathering parameter (χ) for each one of the simulated cases.*

χ \ $\bar{c}_l$	**0**	**0.25**	**0.5**	**0.75**	**1**	**1.5**
0	-0.0037	0.2487	0.4990	0.7523	0.9847	1.4969
0.2	-0.0030	0.2506	0.4989	0.7446	0.9952	1.4956
0.4	-0.0022	0.2493	0.5010	0.7536	0.9981	1.4992
0.5	-0.0017	0.2490	0.5017	0.7506	1.0031	1.5010
0.6	-0.0014	0.2485	0.5002	0.7498	0.9958	1.4997
0.7	-0.0011	0.2497	0.4991	0.7495	0.9982	1.4930
0.8	-0.0007	0.2502	0.4998	0.7508	1.0023	1.4927
1	-0.0001	0.2500	0.5009	0.7572	0.9932	1.4978

Table 4.1: *Exact obtained values of mean lift coefficient ($\bar{c}_l$) for each of the simulated cases.*

χ \ $\bar{c}_l$	**0**	**0.25**	**0.5**	**0.75**	**1**	**1.5**
0	0.0240	0.0079	0.0060	0.0151	0.1019	0.0212
0.2	0.0241	0.0047	0.0086	0.0428	0.0380	0.0356
0.4	0.0231	0.0062	0.0101	0.0373	0.0197	0.0085
0.5	0.0206	0.0109	0.0206	0.0075	0.0358	0.0124
0.6	0.0199	0.0200	0.0027	0.0015	0.0570	0.0048
0.7	0.0180	0.0036	0.0128	0.0070	0.0284	0.1127
0.8	0.0152	0.0055	0.0020	0.0157	0.0418	0.1351
1	0.0023	0.0003	0.0220	0.1776	0.1696	0.0614

Table 4.2: *Exact obtained values of the error in percentaje between the mean lift coefficient ($\bar{c}_l$) achieved in each of the simulated cases and the target ones ($\bar{c}_{ltarget}$).*

The success in the rapid conversion of the simulations, is due to a good estimation of the initial value of the mean pitch angle (θ_m) that is included in the equations of motion (equations 3.3) and adjusted until the desired values of $\bar{c}_l$ are obtained, after an iterative process as it was explained in the previous section of the document. Figure 4.2 shows the required values of θ_m, presented in degrees, to achieve said $\bar{c}_{ltarget}$. The exact values for each simulated case are collected in table 4.3.

As expected, in order to achieve larger values of $\bar{c}_l$, higher values of mean pitch angle are required. Nevertheless, it has to be commented the effect of the feathering parameter in the obtained results. Feathering parameter was defined to be similar to the ratio between pitching and heaving, and in equation 3.10 it was appreciated the direct dependence between feathering parameter and the pitching amplitude (θ_0) so that if one of these parameters increases the same does the other one. On the other hand, in the pitching equation of motion (equation 3.3b), it was seen the independent contribution of mean pitch angle and pitching amplitude to the total pitching motion of the airfoil, although it is assumed that they can not be increased infinitely due to stall reasons. Thus, if one these angles (θ_0 or θ_m) is sufficiently large it has to be compensated with smaller values of the other one. This behaviour is clearly seen looking at figure 4.2, where higher values of mean pitch angle are required at low values of feathering parameter to achieve the desired mean lift coefficient, and as the value of the feathering parameter increases, increasing also the pitching amplitude, the required mean pitch angle becomes smaller. Moreover, it has to be commented the similarity, for all the different cases of $\bar{c}_l$, on the behaviour of θ_m respect to the feathering parameter except for the case of zero lift. In the curves that describe the evolution it has to be recalled a minimum for the cases of $\chi \simeq 0.7$ that coincides with the points of maximum propulsive efficiency, and a maximum at $\chi \simeq 0.5$, points at which maximum thrust is achieved (see figure 4.3 and figure 4.4).

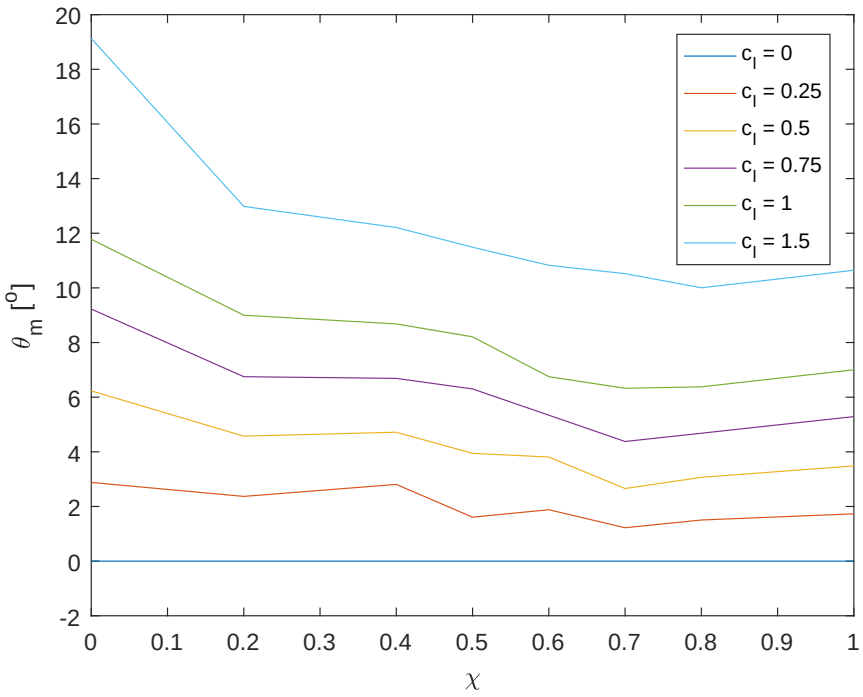

Figure 4.2: *Mean pitch angle (θ_m [^{o}]) as a function of feathering parameter (χ) for each one of the simulated cases.*

χ \ $\bar{c}_l$	**0**	**0.25**	**0.5**	**0.75**	**1**	**1.5**
0	0	2.8790	6.2308	9.2252	11.7795	19.1275
0.2	0	2.3691	4.5746	6.7500	9.0000	12.9823
0.4	0	2.8074	4.7175	6.6883	8.6815	12.2095
0.5	0	1.6075	3.9442	6.3015	8.2089	11.4889
0.6	0	1.8811	3.8103	5.3414	6.7501	10.8273
0.7	0	1.2214	2.6563	4.3782	6.3263	10.5213
0.8	0	1.5046	3.0671	4.6805	6.3784	10.0035
1	0	1.7309	3.4843	5.2894	7.0030	10.6459

Table 4.3: *Exact obtained values of mean pitch angle (θ_m [^{o}]) for each of the simulated cases.*

One of the objectives of the present project was to find a combination for the values of the parameters involved in the kinematics of the airfoil, to achieve maximum values of thrust. Table 4.4 collects the exact obtained values of $\bar{c}_t$ after the postprocessing of data provided by TUCAN for each of the simulated cases.

Moreover, these results are also shown in figure 4.3, where it is appreciated how the lower the desired lift, the higher the thrust that can be generated. It has to be recalled the fact that at certain values of χ there is no generation of thrust, as it occurs for values of χ larger than $0.8 \sim 0.9$, depending of the case analyzed, and for $\bar{c}_l = 1.5$ due to the large value of lift, thrust is not generated until a value of feathering $\chi \simeq 0.1$ is achieved. Furthermore, it is clearly seen how maximum values of mean thrust coefficient are achieved at values of feathering parameter between 0.5 and 0.6.

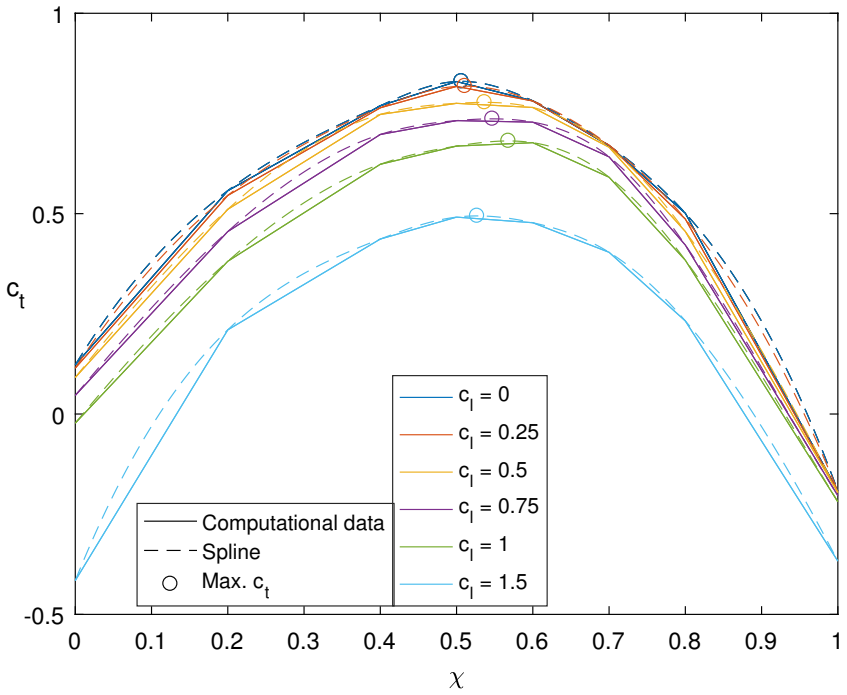

Figure 4.3: *Calculated and approximated values of mean thrust coefficient ($\bar{c}_t$) as a function of feathering parameter (χ) for each one of the simulated cases, and maximum values of $\bar{c}_t$ for each $\bar{c}_l$.*

The fact of launching new simulations in TUCAN to obtain the exact value of χ that provides maximum thrust is not complex but tedious, and the accuracy of the exact values does not compensate the computational time required, and the associated cost to achieve them. Thus, an approximation of the values of $\bar{c}_t$ that would be obtained at every single χ is include in figure 4.3, where the points of maximum thrust are remarked. Table 4.5 collects the approximated values of χ for maximum thrust. To ensure the validity of the approximation made, the error between the maximum obtained thrust coefficient in the simulations for each $\bar{c}_l$

case and the maximum approximated value of thrust coefficient is calculated as follows:

$$Error_{max,\bar{ct}} = \left| 100 - \frac{\bar{c}_{tmax,\bar{c}_l} \cdot 100}{\bar{c}_{t,approx}} \right| \tag{4.1}$$

χ \ $\bar{c}_l$	**0**	**0.25**	**0.5**	**0.75**	**1**	**1.5**
0	0.1226	0.1145	0.0911	0.0464	-0.0227	-0.4155
0.2	0.5573	0.5454	0.5108	0.4553	0.3811	0.2099
0.4	0.7692	0.7641	0.7475	0.6975	0.6231	0.4366
0.5	0.8297	0.8175	0.7753	0.7322	0.6686	0.4913
0.6	0.7815	0.7810	0.7649	0.7283	0.6770	0.4773
0.7	0.6696	0.6707	0.6656	0.6416	0.5909	0.4035
0.8	0.5010	0.4865	0.4554	0.4216	0.3837	0.2322
1	-0.19214	-0.1930	-0.1959	-0.2038	-0.2190	-0.3670

Table 4.4: *Exact obtained values of mean thrust coefficients ($\bar{c}_t$) for each of the simulated cases.*

$\bar{c}_l$	**0**	**0.25**	**0.5**	**0.75**	**1**	**1.5**
χ_{approx}	0.5066	0.5110	0.5369	0.5471	0.5681	0.5271
$\bar{c}_{tapprox}$	0.8301	0.8182	0.7777	0.7365	0.6814	0.4943
Error [%]	0.0387	0.0818	0.3039	0.5903	0.6394	0.6056

Table 4.5: *Approximated values of maximum thrust ($\bar{c}_t$) for each mean lift coefficient ($\bar{c}_l$) studied and the corresponding feathering parameter (χ) to achieve them.*

It has been obtained a maximum error of 0.63% for the case of $\bar{c}_l = 1$, so the approximation made can be considered good enough. The values of the errors obtained for the rest of lift coefficient cases, are also included in table 4.5. Moreover, looking at said figure and tables it can be seen how larger values of thrust are achieved at lower values of lift, and how the tendency of the values of χ, at which these maximum values are achieved, is to increase as lift is increased up to a point between $\bar{c}_l = 1$ and $\bar{c}_l = 1.5$ where the value of the required feathering parameter to achieved maximum thrust decreases. Furthermore, it exits a trade off between the desired lift and the maximum thrust generated, existing a difference of 40.45 % between the maximum $\bar{c}_t$ generated at $\bar{c}_l = 0$ and $\bar{c}_l = 1.5$. From a propulsion

point of view, the results obtain for $\bar{c}_l = 0.25$ ($\bar{c}_l = 0$ does not make sense from an aerodynamic point of view since there is no generation of lift and the results obtained for that $\bar{c}_l = 0.25$ does not differ a lot from the ones of $\bar{c}_l = 0$) are excellent. Nevertheless, in some circumstance the weight that the flying machine has to carry is larger, and a balance between the payload allowed and the thrust generated has to be done. Looking at the results obtained, it can be conclude that the optimum point is to achieve values of $\bar{c}_l$ of the order of 1 (even slightly higher) without penalizing a lot the generation of thrust (that differs in a 17.9% to the thrust achieved at $\bar{c}_l = 0$).

To find the combination of parameters to obtain the best results in terms of propulsive efficiency was one of the main objectives of the project. Knowing the exact values of the parameters involved in the kinematics of the airfoil for each simulated case and the aerodynamic forces obtained, applying equation 3.17 the exact values of propulsive efficiency are obtained for each one of the 48 cases launched in TUCAN. These values are collected in table 4.6, and they are also presented in figure 4.4.

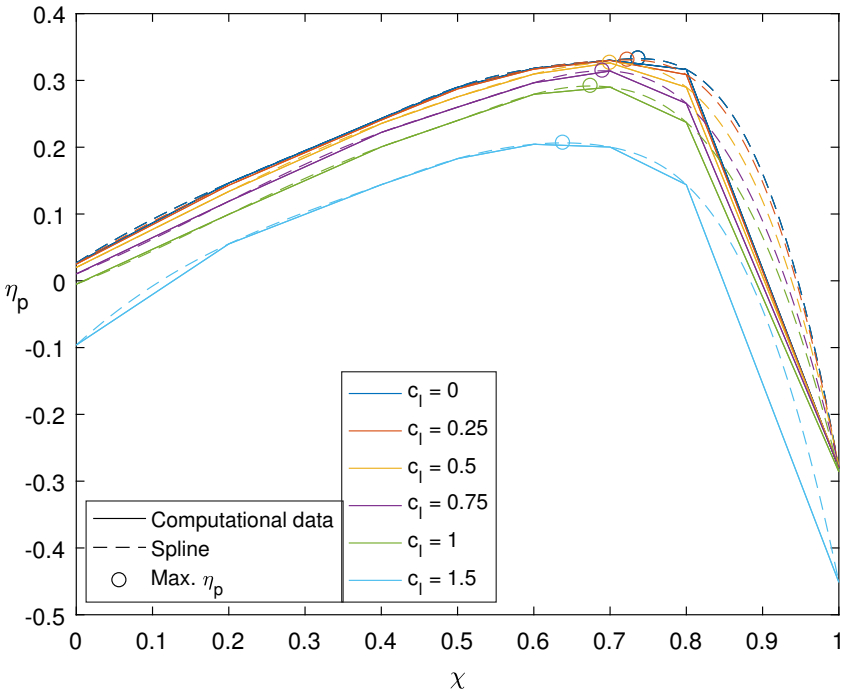

Figure 4.4: *Calculated and approximated values of propulsive efficiency (η_p) as a function of feathering parameter (χ) for each one of the simulated cases and maximum values of η_p for each $\bar{c}_l$.*

χ \ $\bar{c}_l$	**0**	**0.25**	**0.5**	**0.75**	**1**	**1.5**
0	0.0267	0.0250	0.0200	0.0102	-0.0050	-0.0961
0.2	0.1463	0.1430	0.1337	0.1190	0.0995	0.0551
0.4	0.2429	0.2407	0.2355	0.2221	0.2005	0.1439
0.5	0.2899	0.2872	0.2754	0.2599	0.2400	0.1829
0.6	0.3180	0.3169	0.3095	0.2964	0.2792	0.2044
0.7	0.3302	0.3299	0.3261	0.3141	0.2899	0.2002
0.8	0.3163	0.3087	0.2898	0.2656	0.2372	0.1438
1	-0.2808	-0.2799	-0.2771	-0.2781	-0.2859	-0.4514

Table 4.6: *Exact obtained values of propulsive efficiency (η_p) for each of the simulated cases.*

Looking at figure 4.4, it can be appreciated how as feathering parameter is increased the same does the propulsive efficiency in a similar way to the behaviour of $\bar{c}_t$ previously commented and showed in figure 4.3, since η_p is proportional to it. Thus, as it occurs in the analysis of the mean thrust coefficients obtained, there are values of feathering parameter for which the propulsive efficiency obtained is negative. Once again, coinciding with the case of $\bar{c}_t$, for values of χ larger than $0.8 \sim 0.9$, depending on the analyzed case, the values of η_p abruptly decrease from almost their maximum values, and negative values are obtained, as well as for the case of $\bar{c}_l = 1.5$, where the efficiency obtained is negative up to $\chi = 0.1$. Moreover, it has to be commented the presence of maximum values of propulsive efficiency although in this case, they are obtained at values of χ between 0.6∼0.7 and the curve in the behaviour of η_p as a function of χ seems to be pushed to the right (respect to the results obtained in terms of $\bar{c}_t$) due to the influence of other parameters such as the lift force, heaving and pitching rates, that influence in the calculation of η_p (see equation 3.17). As it occurred for the case of maximum thrust, the fact of launching new simulations in TUCAN to achieve the exact values of feathering parameter at which maximum propulsive efficiency is achieved, does not compensate the computational cost. Thus, an approximation is performed in a similar way as in the previous case and the results obtained are also included in figure 4.4. The estimated values of χ at which maximum η_p would be achieved are collected in table 4.7. To ensure the validity of the approximation made, once again, the error between the approximated maximum values and the actual values obtained in the simulation is computed as follows:

$$Error_{max,\eta_p} = \left| 100 - \frac{\eta_{p,max,\bar{c}_l} \cdot 100}{\eta_{p,approx}} \right| \tag{4.2}$$

$\bar{c}_l$	**0**	**0.25**	**0.5**	**0.75**	**1**	**1.5**
χ_{approx}	0.7372	0.7230	0.7000	0.6903	0.6746	0.6385
$\eta_{p_{approx}}$	0.3326	0.3308	0.3262	0.3144	0.2916	0.2065
Error [%]	0.7098	0.2509	0.0000	0.0895	0.5785	0.9977

Table 4.7: *Approximated values of maximum propulsive efficiency (η_p) for each mean lift coefficient ($\bar{c}_l$) studied and the corresponding feathering parameter (χ) to achieve them.*

The results obtained are also collected in table 4.7. In this case, the maximum error obtained is of 0.99% for the case of $\bar{c}_l = 1.5$. Looking at said figure and tables, it can be seen how for the lower the lift achieved the higher the thrust that can be generated and thus, the higher the propulsive efficiency obtained. Moreover, it has to be commented how as lift is increased the value of feathering parameter at which maximum η_p is achieved decreases. Again, it exists a trade off between the lift and propulsive efficiency obtained. In this case the difference between the maximum propulsive efficiency achieved at $\bar{c}_l = 0$ and $\bar{c}_l = 1.5$ is of 37.91%. Looking at figure 4.4 and table 4.7, it is clearly apreciated how this difference is much smaller between a $\bar{c}_l l = 0$ and $\bar{c}_l = 1$ differing only in a 12.32%. Thus, the optimum is to flight at lift coefficients of the order of 1 or slightly larger, where the propulsive efficiency is almost penaliced.

In order to find the optimum envelope in terms of parameters that provides the combination of kinematic parameters to achieve the best results according to lift force, thrust force and propulsive efficiency, the results previously commented of η_p are presented as a function of $\bar{c}_t$ on figure 4.5. On said figure, the values of feathering parameter for maximum generation of thrust and maximum propulsive efficiency ($\chi = 0.5$ and $\chi = 0.7$ respectively) are also shown for each one of the 6 different lift cases studied along the project. Looking at said figure, and without forgetting the estimation made of the points of maximum $\bar{c}_t$ (figure 4.3 and table 4.5) and maximum η_p (figure 4.4 and table 4.7), it can be clearly seen how the optimum feathering parameter to flight without almost penalize the generation of $\bar{c}_t$ or η_p is in almost all the cases at $\chi \simeq 0.6$. It has to be also commented, the fact that all the curves looks like very similar, and the results obtained in terms of $\bar{c}_t$ and η_p are quite the same for all the cases of mean lift coefficient studied except for $\bar{c}_l = 1.5$, where a clear difference is appreciated. Nevertheless, this difference is more than justify since the larger values of lift are always penalized with a less generation of thrust and thus, taking into account the contribution of this two forces, propulsive efficiency is penalized obtaining lower values.

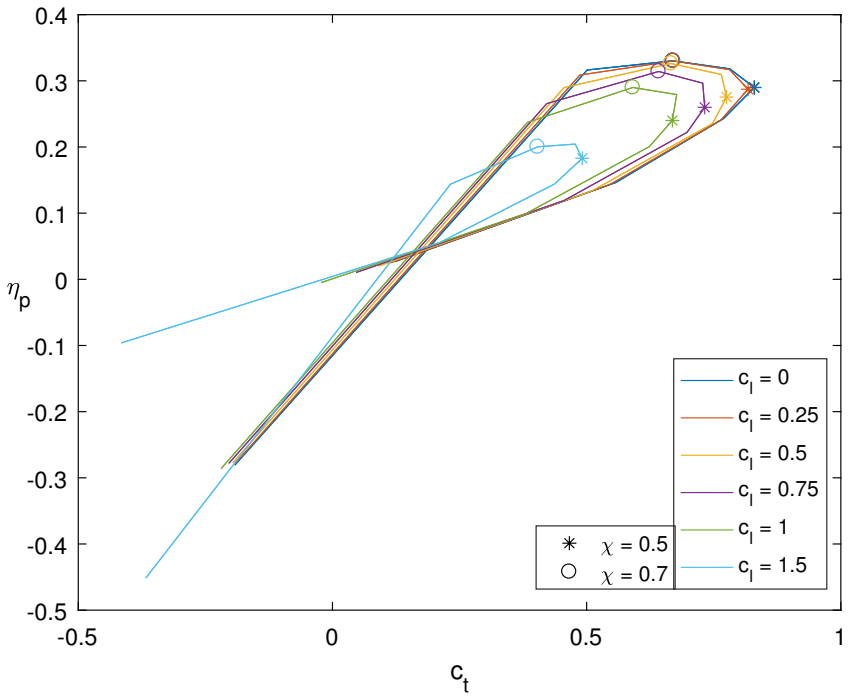

Figure 4.5: *Propulsive efficiency (η_p) as a function of mean thrust coefficient ($\bar{c}_t$) for each one of the mean lift coefficients ($\bar{c}_l$) studied. Values of feathering parameter (χ) for maximum generation of thrust and maximum propulsive efficiency are also included.*

In next section (section 4.2) it is presented the behaviour followed by the vorticities around the flow in a period of time, for the most relevant cases. The LEV and TEV are the two main vortical structures in the flow responsible of the generation of forces. Thus, in the next figures, it is previously presented the temporary history of c_l and c_t for a period of time.

Figure 4.6 presents the temporary history of c_l for each one of the 6 different values of $\bar{c}_l$ studied, for the most relevant values of feathering parameter, so that it is included $\chi = 0$ and $\chi = 1$, since pure heaving motion and a smooth motion respect to the flow are respectively presented, and $\chi = 0.5$ and $\chi = 0.7$ since at these values, maximum generation of thrust and maximum propulsive efficiency are respectively obtained. In the figure, the part with the white background corresponds to the downstroke motion and the one with the light grey corresponds to the upstroke. Looking at said figure, it can be appreciated how the lower the value of feathering parameter the larger the amplitude of c_l. Feathering parameter is responsible of the orientation of the airfoil respect to the incoming velocity, taking an important role in the magnitude of the forces generated and their orientation. Moreover, these forces are larger during the downstroke than

in the upstroke.

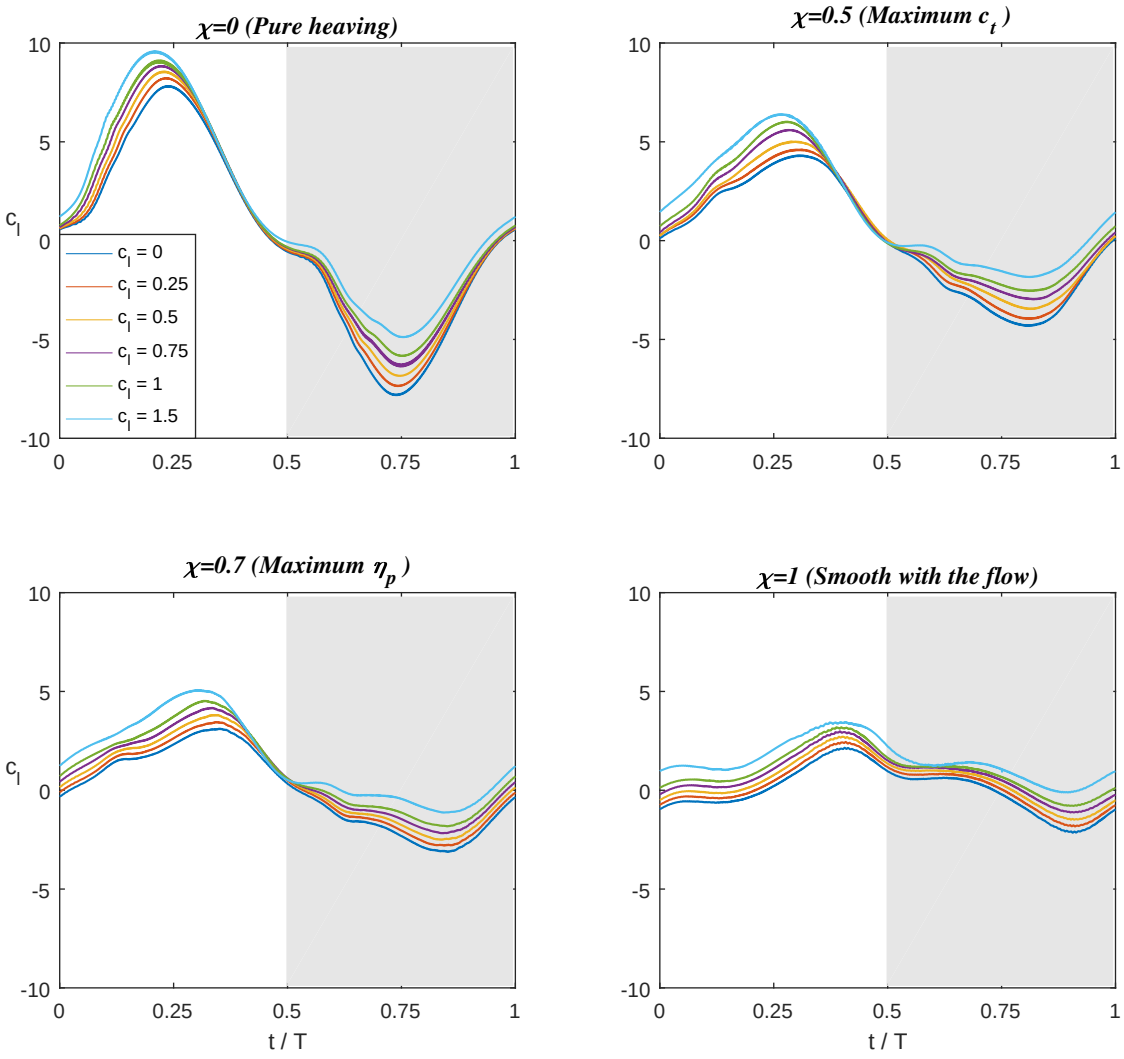

Figure 4.6: *Temporary history of c_l in one period of motion for the most relevant values of χ for each one of the six different cases of $\bar{c}_l$.*

Figure 4.7 shows a clear comparison on the forces achieved at each studied value of feathering parameter for the cases of lowest and highest value of $\bar{c}_l$. There, the behaviour of larger forces appearing for the larger values of χ is appreciated. Moreover, it is seen how as the value of $\bar{c}_l$ is increased larger forces takes place during the downstroke while for the case of $\bar{c}_l = 0$ larger forces takes place along the upstroke.

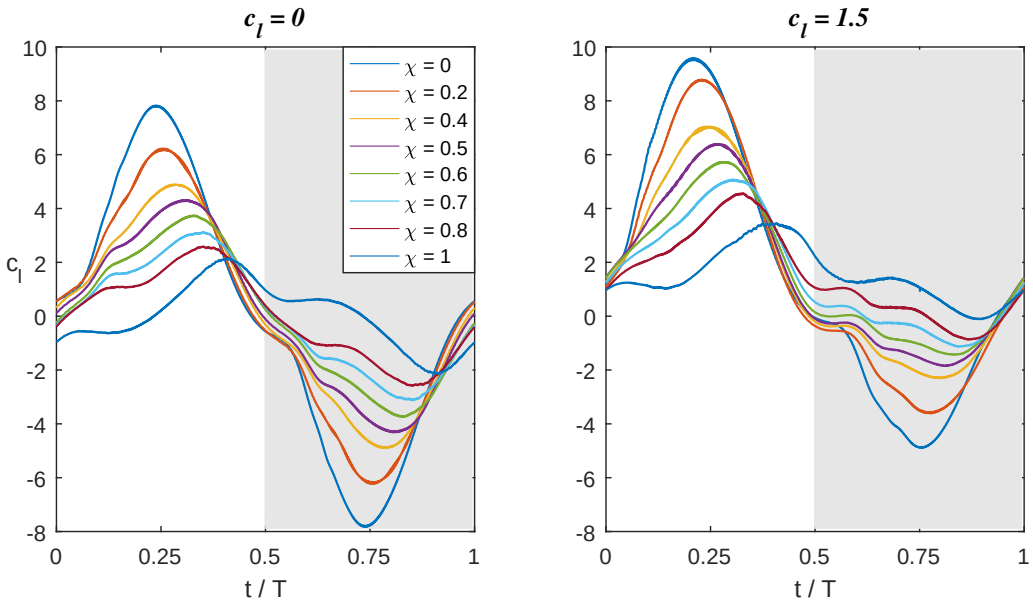

Figure 4.7: *Temporary history of c_l for the highest and lowest values of $\bar{c}_l$ for each one of the eight different cases of χ studied.*

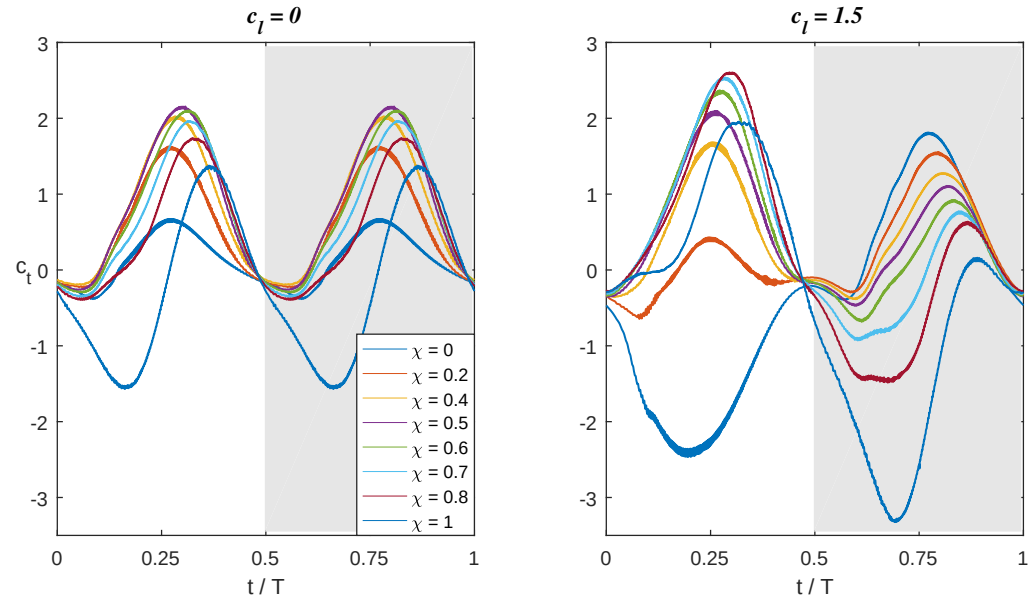

Figure 4.8: *Temporary history of c_t for the highest and lowest values of $\bar{c}_l$ for each one of the eight different cases of χ.*

Differently to the results presented in figure 4.6 and figure 4.7, the results obtained in terms of thrust coefficient, shown in figure 4.8 and 4.9, are more unpredictable. Looking at figure 4.9, it can be seen how the temporary history of this force is not

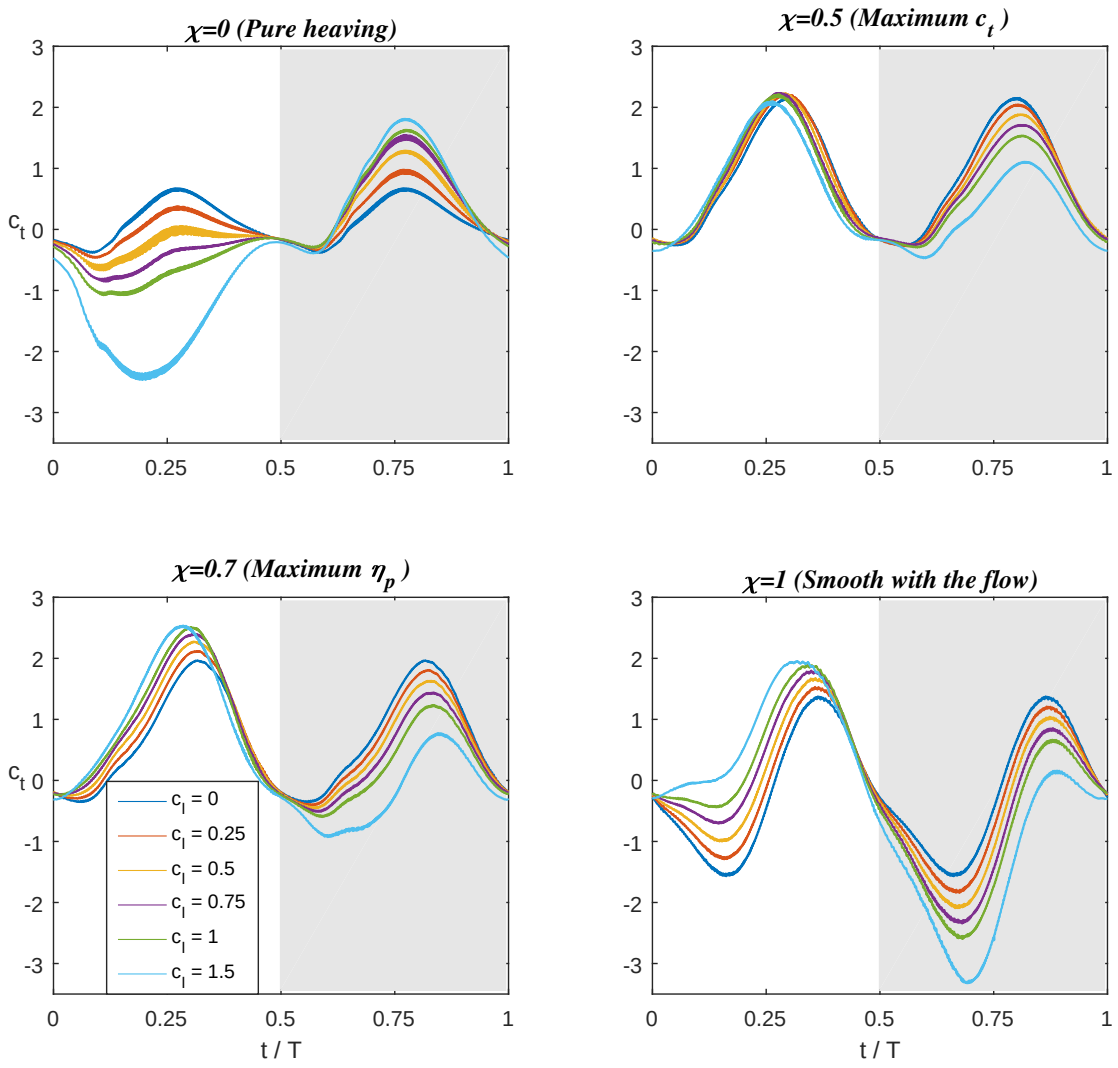

Figure 4.9: *Temporary history of c_t in one period of motion for the most relevant values of χ for each one of the six different cases of $\bar{c}_l$.*

symmetric during the downstrock and upstroke. It is seen how for lower values of χ, higher values of thrust are obtained along the upstroke, while as χ is increased higher values are obtained in the downstroke. In these figures, it can be seen how at $\chi = 0.5$ the temporary history of c_t presents positive values of thrust coefficient along almost the whole period, allowing to achieve maximum values of generated thrust. On the other hand, it has to be remarkable the behaviour presented at $\chi = 1$ where larger negative values takes place along the upstroke that can not be compensated with the positive ones yielding to the negative values of $\bar{c}_t$ previously commented on figure 4.3.

4.2 Flow visualization

Having seen the temporary history of lift and thrust coefficients for a period of motion, in this section a visualization of the flow is presented, in order to relate the effect that LEV and TEV have on the generation of these forces.

In the following figures, the visualization of the flow along a period is presented in four snapshots for the most relevant cases studied. First of all, it is presented a comparison between the cases of lowest and highest values of $\bar{c}_l$ studied ($\bar{c}_l$=0 and $\bar{c}_l$=1.5) for a pure heaving motion ($\chi = 0$) and a motion that is smooth with the flow (χ=1). After that this comparison is made with the same values of mean lift coefficient but at the interest values of feathering parameter in terms of maximum generation of thrust and maximum propulsive efficiency, which are $\chi = 0.5$ and $\chi = 0.7$ respectively.

Looking at figure 4.10 and figure 4.11, it can be seen how at $\chi = 1$ the airfoil moves smoothly in the flow without generating almost any force. Nevertheless, at $\chi = 0$ pure heaving motion is observed, and as expected larger forces are presented. It can be seen the effect of the LEV and TEV and how they dissipate in the wake. The effect of these vortical structures is even more larger for the case of $\bar{c}_l = 1.5$ as it can be seen in figure 4.11. Moreover, looking at both figures it can be see how at $t = 0.75T$, coinciding with the upstroke, there is a creation of a LEV in the bottom part of the airfoil and the detachment of the vortex generated in the upper part that causes a momentary lose of the list force, and at $t = 0.25T$ during the downstroke this LEV is generated in the upper part and the detachment of the TEV, being the responsible of the higher values of c_l seen in its temporary history.

Figure 4.12 and figure 4.13 show the behaviour of the flow at values of feathering parameter of 0.5 and 0.7 coinciding with maximum generation of thrust and maximum propulsive efficiency. Although small differences are presented between them, it can be seen how for $\chi = 0.5$ larger forces takes place around the airfoil, and these forces become stronger at $\bar{c}_l = 1.5$. During the upstroke, at $t = 0.25T$ it is seen how the TEV is much stronger at $\chi = 0.5$ as well as the LEV generated during the downstroke.

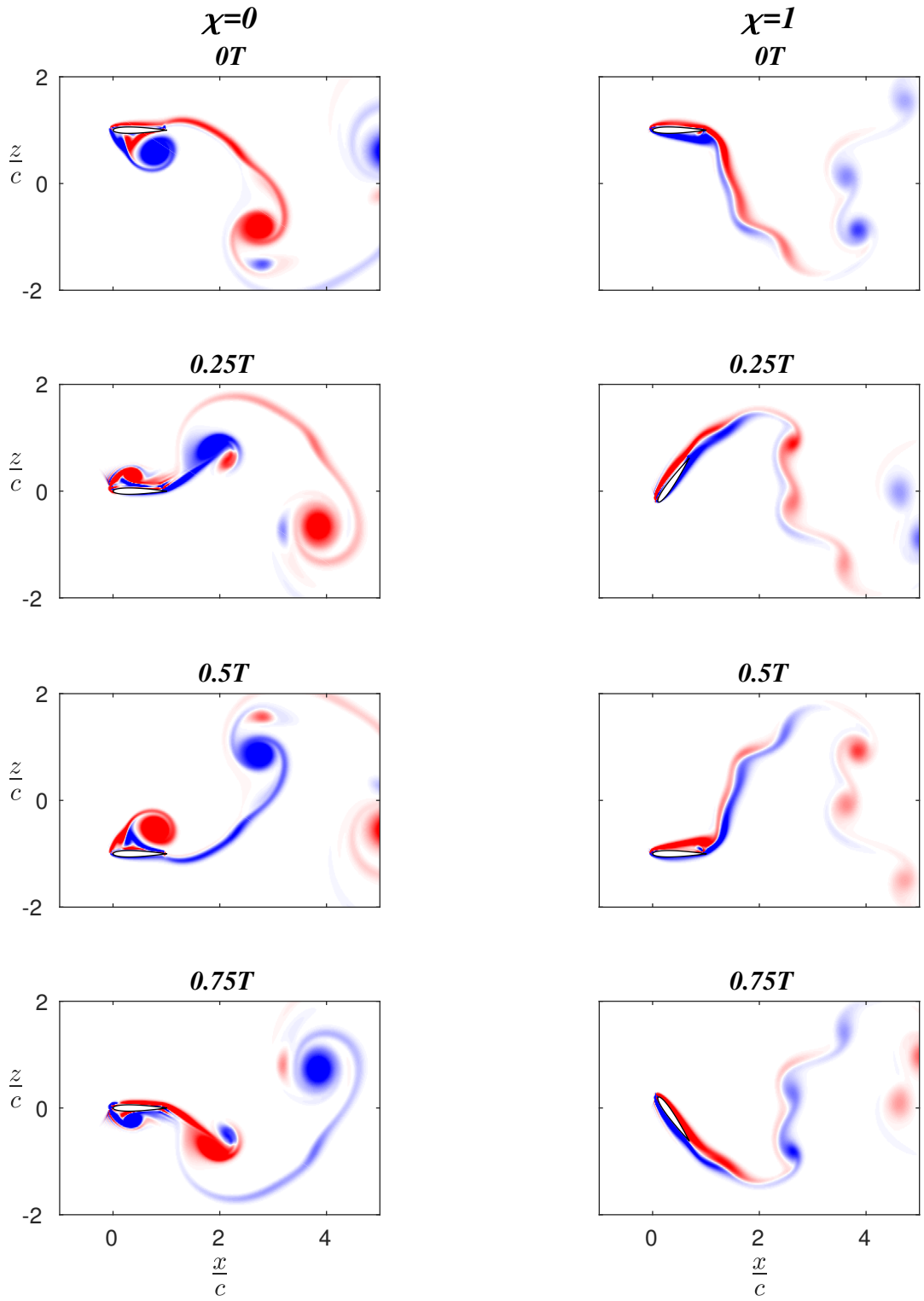

Figure 4.10: *Flow visualization for the case of $\bar{c}_l = 0$ along a period of motion for pure heaving motion ($\chi = 0$) and a motion smooth with the flow ($\chi = 1$).*

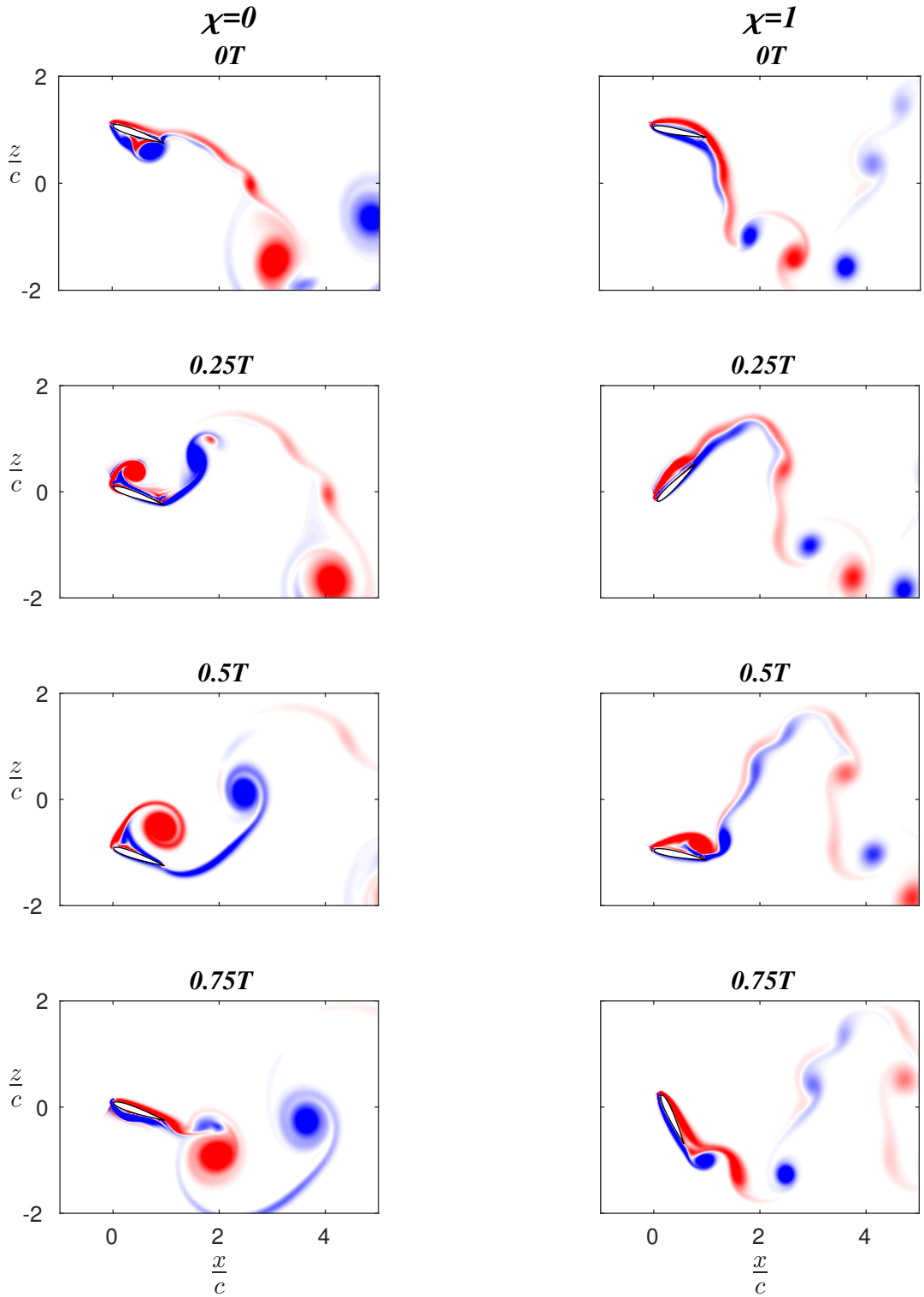

Figure 4.11: *Flow visualization for the case of* $\bar{c}_l = 1.5$ *along a period of motion for pure heaving motion* ($\chi = 0$) *and a motion smooth with the flow* ($\chi = 1$)

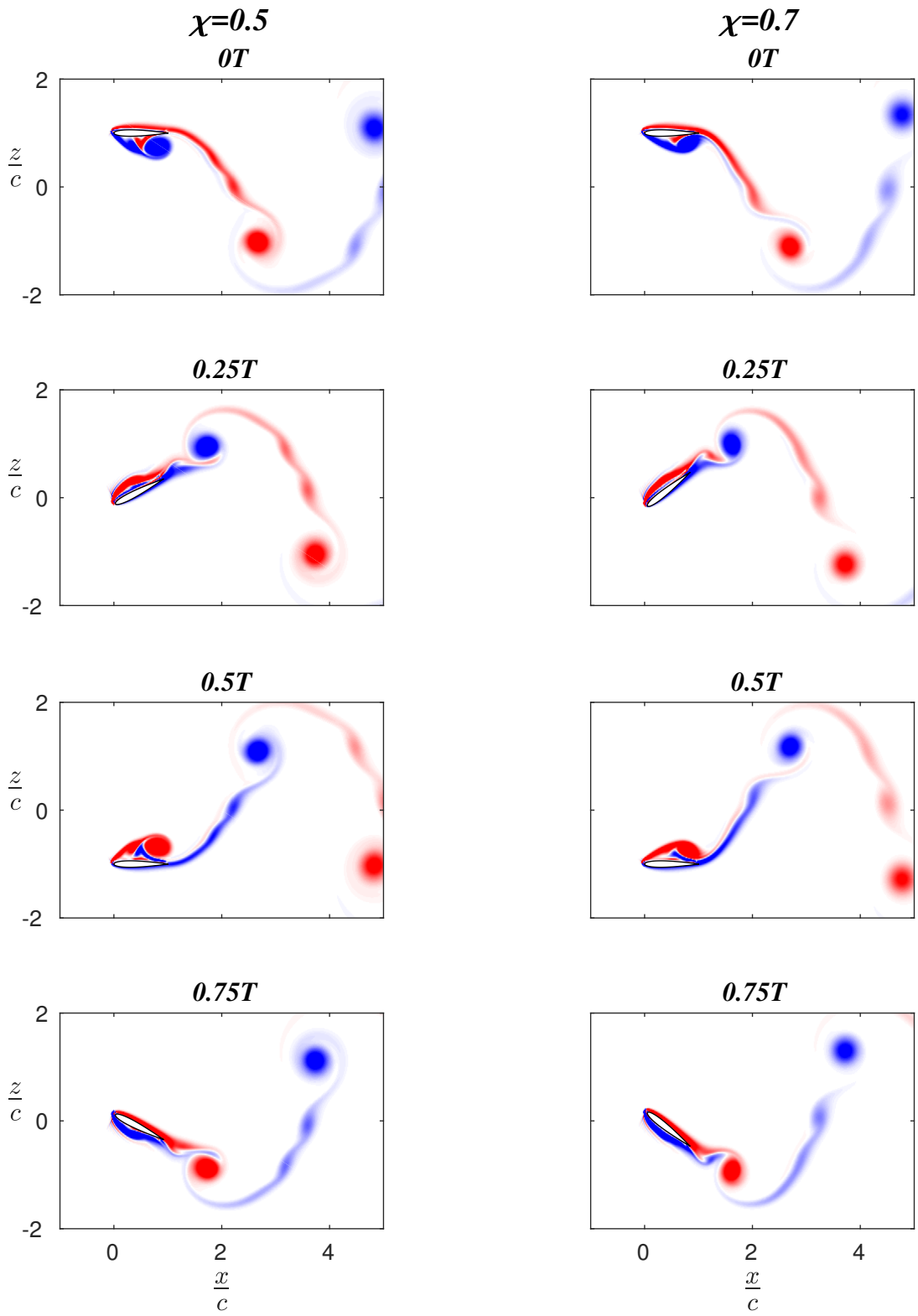

Figure 4.12: *Flow visualization for the case of* $\bar{c}_l = 0$ *along a period of motion for values of feathering parameter of maximum generation of thrust* ($\chi = 0.5$) *and maximum propulsive efficiency* ($\chi = 0.7$)

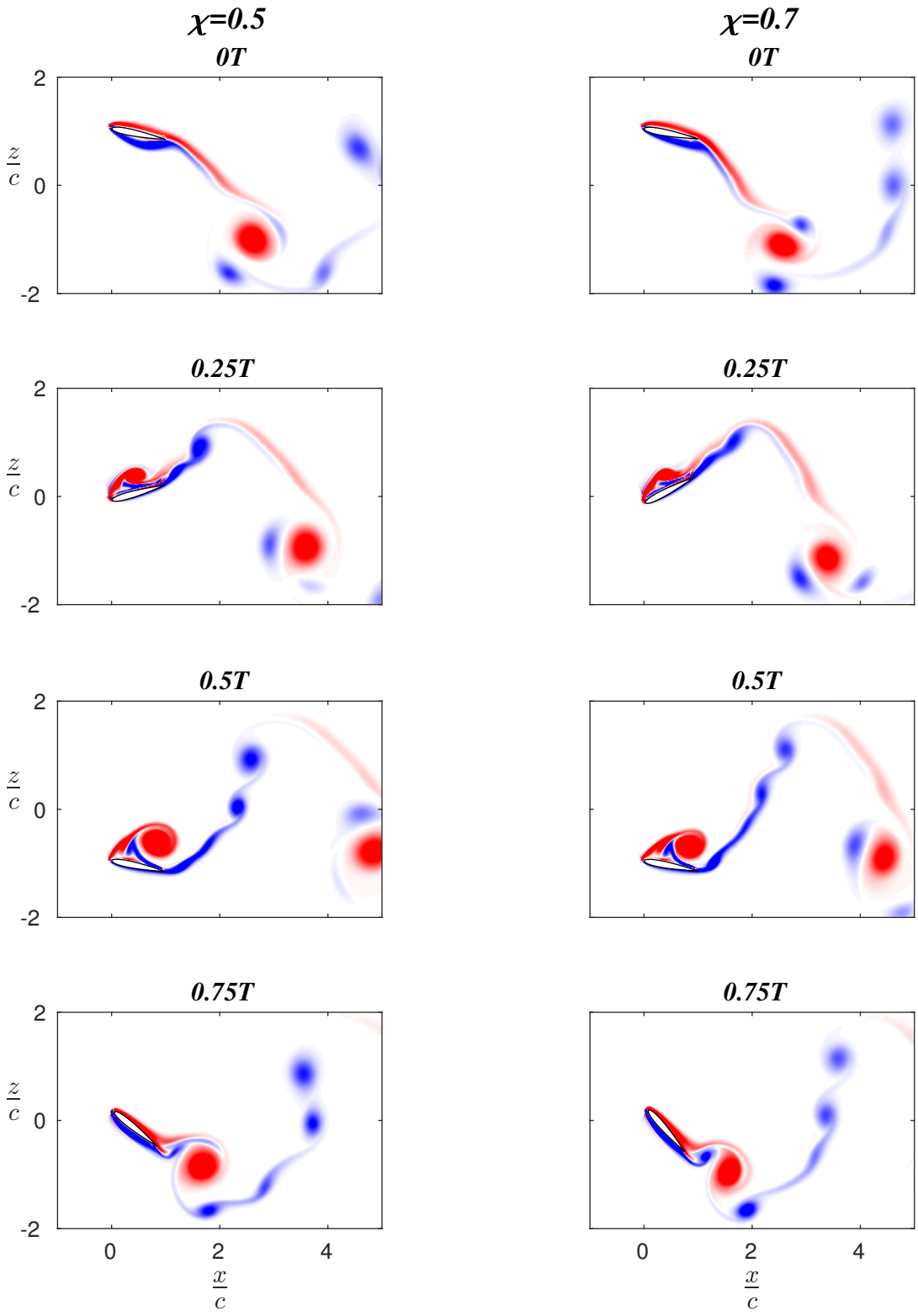

Figure 4.13: *Flow visualization for the case of* $\bar{c}_l = 1.5$ *along a period of motion for values of feathering parameter of maximum generation of thrust* ($\chi = 0.5$) *and maximum propulsive efficiency* ($\chi = 0.7$)

4.3 Comparison of results with a parallel project

In this section, it is included a comparison between the results obtained in section 4.1 and the ones obtained in Yuste 2017, a companion project.

4.3.1 Numerical method

In Yuste 2017 it can be found a validation of reduced order of the method used by Moriche 2017. This new model consist on a simplification of the equations that describe the aerodynamic forces, and whose objective is to reach a high efficient tool in terms of computational time, although a small gap of error has to be included in the results. This model has been developed based on the cases detailed in Moriche 2017, and the objective of said project is to check the validity of the model using cases that differs to these ones.

In order to compute the aerodynamic forces, the model is based in the Navier Stokes equations for an incompressible case. In order to obtain the simplified expression of the forces, the model follows the Chang algorithm, explained in detail in Chang 1992, where forces are obtained by a sum of several integral terms. Thus, the normal components of forces are calculated as follows:

$$F_x = -\rho \int_S \frac{\phi_x}{U_\infty} \frac{\partial \vec{u}}{\partial t} \cdot \vec{n} dS + \frac{\rho}{2} \int_S |\vec{u}|^2 \vec{n} \cdot \vec{e_x} dS - \rho \int_V (\vec{u} \times \vec{\omega}) \cdot \frac{\nabla \phi_x}{U_\infty} dV + \mu \int_S (\vec{\omega} \times \vec{n}) \cdot \left(\frac{\nabla \phi_x}{U_\infty} + \vec{e_x} \right) dS \tag{4.3a}$$

$$F_z = -\rho \int_S \frac{\phi_y}{U_\infty} \frac{\partial \vec{u}}{\partial t} \cdot \vec{n} dS + \frac{\rho}{2} \int_S |\vec{u}|^2 \vec{n} \cdot \vec{e_z} dS - \rho \int_V (\vec{u} \times \vec{\omega}) \cdot \frac{\nabla \phi_y}{U_\infty} dV + \mu \int_S (\vec{\omega} \times \vec{n}) \cdot \left(\frac{\nabla \phi_z}{U_\infty} + \vec{e_z} \right) dS \tag{4.3b}$$

Different contributions take part in the calculation of the components of the forces. In equations 4.3a and 4.3b, four different integral terms can be distinguish. The first two terms make reference to the forces produced by the body motion, the third integral component refers to the flow vorticity, and the last integral term to the surface vorticity. These three different contributions to the total force, exerted by the fluid into the body, have different importance and relevance into the total force. In the next paragraphs, these contributions and how their calculation is achieved, is developed.

The two integral terms corresponding to the body motion forces include all the forces caused by the movement of the airfoil inside the fluid domain. The potential that defines this force contribution depends directly on the geometry and the kinematics of the problem. Thus, this is a highly reliable contribution that can not be considered as a source of error. The potential is complex to be calculated, and it is given by solving the Laplace equation for the airfoil.

On the other hand, the flow vorticities considered in the third term is the contribution that represents the highest source of error. This is the term to be simulated in the model, where different simplifications have been considered. There, the circulation of the flow (Γ), and the direction of the force, take an important role. Kutta-Joukowski established that $F = \rho U_{infty} \times \Gamma$ so that the incident velocity and the force were perpendicular. Nevertheless, looking at the simulated cases collected in Moriche 2017, it is easy to observe how the components of the force are not perpendicular to the incident velocity but to the chord of the airfoil. Although this behaviour in the direction of the forces is not fulfill in the whole period, it is done in almost the totality of the period. The difference respect to what Kutta-Joukowski established, is that this theory was applicable for flows around rigid wings, and wings have evolved with the past of the years being more flexible and introducing changes in their shape. Despite of this, the scalar formula of the Kutta-Joukowski formula, is kept ($\left|\vec{F}\right| = \rho\Gamma\left|\vec{U}\right|$). To solve the problem, the circulation is calculated by means of a constant fitting model of Pesavento and Wang 2004. The formula used in the calculation of the circulation is composed by a translational and rotational terms, and it is given by:

$$\Gamma = \Gamma_T + \Gamma_R = \frac{1}{2} G_T c \left|\vec{U}\right| sin\left(2\alpha_e\right) + \frac{1}{2} G_R c^2 \dot{\theta} \tag{4.4}$$

where, G_T and G_R are the two constants that represent the translational and rotational terms respectively. The rotational constant is calculated by similarity with the expression of the potential thin airfoil theory, where:

$$\Gamma_R = \pi c^2 \dot{\theta} \left(\frac{3}{4} - \frac{x_p}{c}\right) \tag{4.5}$$

Being the pivoting point located at the quarter chord and by similarity, it is conclude that $G_R = \pi$. The G_T constant is calculated, ones G_R is defined, by means of a fitting method explained with more detail in Yuste 2017, yielding in a final value of $G_T = 1.85$. The fact of using this constant in the calculation of the total Γ represents a possible source of error once they are used out of the base cases to develop the model. Thus, these constants need a continuous checking and modifications for each one of the different cases in order to diminish as much as possible the source of error.

Finally, the fourth integral term corresponding to the forces produced by the vorticities generated by the surface of the body. This final contribution to the total force, is very small compared with the others, and its calculation is tedious. Thus, in order to simplify the model given in Moriche 2017 it has been decided to neglect the contribution of this term. As a consequence, a small source of error produced by this decision has to be considered.

With the model already developed and using the equations of motion (equations 3.3), in Yuste 2017, it can be found the analysis of multiple cases, performed in Matlab, where different parameters involved in the kinematics of the airfoil, the Reynolds number and pivoting point position between others, have been varied in order to find possible patrons in the behaviour of the simulations and determine for which cases the model works providing good results.

Due to the high efficiency of the method in terms of computational time, all the simulations included in this document were also analyzed. Thus, in the following pages it is presented a comparison between the results obtained in this project performing the Direct Numerical Simulations using TUCAN, and the results provided using the simplified model previously commented. To make the comparison possible all the necessary data regarding the computational domain, boundary conditions and every single parameter involved in the kinematics of the airfoil for each of the 48 different cases studied, is provided to perform the analysis using this model. The results obtained are presented in section 4.3.2.

4.3.2 Results

Taking into account that TUCAN is sufficiently validated, this section aims to find for which cases the results obtained using the proposed simplified model are good enough, although some differences in the results obtained are expected due to the assumptions and simplifications made.

Figure 4.14 shows a comparison on the behaviour of the mean lift coefficient as a function of feathering parameter between the results obtained using TUCAN and the simplified method in study. The difference in the results is notorious. In the first computational method the mean pitch angle is continuously varied until the desired mean lift coefficient is achieved providing accurate results as it can be appreciated. Nevertheless, in the second one, the final values of θ_m to achieve those $\bar{c_l}$ values and other kinematic parameters are introduced in the equations of motion (3.3) and the aerodynamic forces are directly calculated, as explained in section 4.3.1, by means of the equations 4.3 yielding to results that differ a lot to the expected ones.

It can be observed how at $\chi = 0$ a value of $\bar{c_l} \simeq 0.05$ is obtained no matter the value of the mean pitch angle imposed. As feathering parameter increases larger values of mean lift coefficient are obtained until those values converge at $\chi \simeq 0.7$

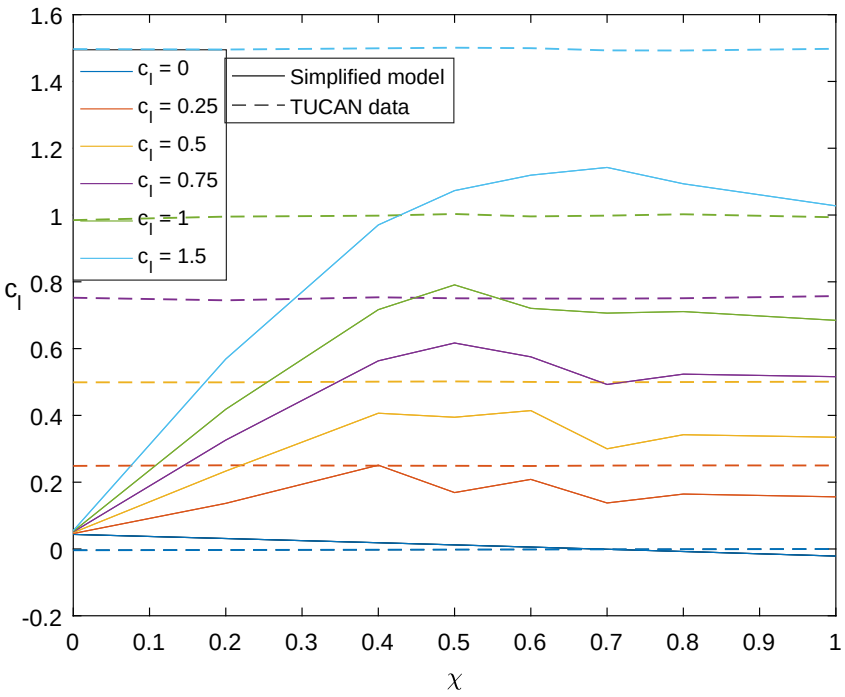

Figure 4.14: *Comparison of the mean lift coefficients ($\bar{c}_l$) obtained using TUCAN and a simplified model for each one of the simulated cases.*

to a value of mean lift coefficient that differs in approximately a 30 % to the expected value. The fact of obtaining these differences in values can be explained due to the assumptions made while computing the forces components. In section 4.3.1 it is explained how in the third integral term corresponding with the vorticity of the flow, the translational and rotational constants are estimated supposing a high source of error. Moreover the direction of the normal components of the forces respect to the incoming velocity and the chord of the airfoil represents and important role in the calculation. This added with the small contribution to the total error derived from neglecting the force produced by the vorticities caused by the surface of the airfoil (fourth integral term), can explained how the final lift force achieved is smaller than the expected one. Furthermore, the fact of achieving such lower values of lift for values of χ between 0 and 0.4 could be explained due to the effect exerted by the LEV and its principal contribution to the final lift force.

Regarding the mean thrust coefficient, the results provided using the simplified model are similar to the ones of TUCAN. Looking at figure 4.15, it can be appreciated how the behaviour of the curve followed by each of the target lift coefficient cases behaves similar to what it was expected. Nevertheless, the curve seems to

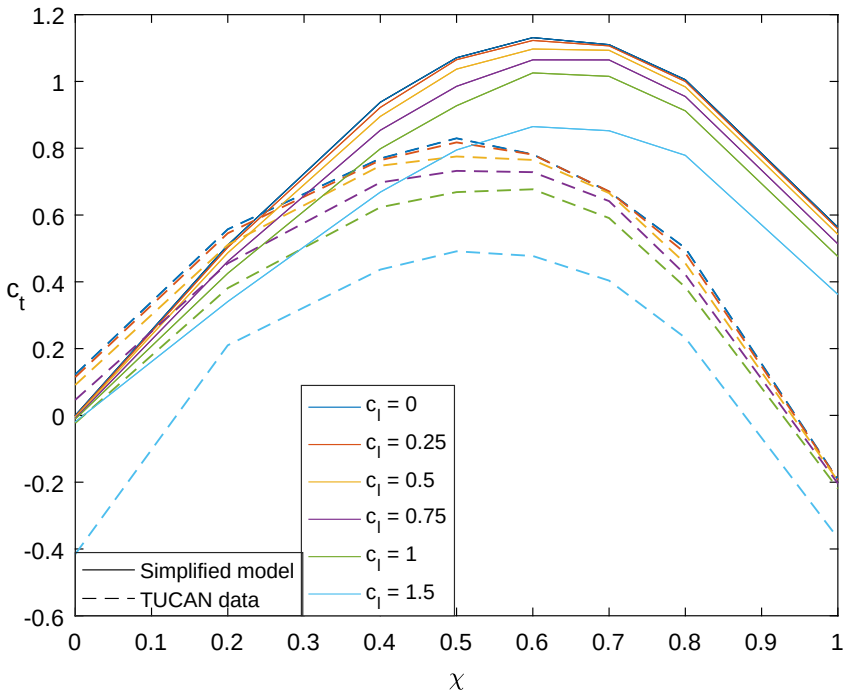

Figure 4.15: *Comparison of the mean thrust coefficients ($\bar{c}_t$) obtained using TUCAN and a simplified model for each one of the simulated cases.*

be pushed up and to the left, achieving larger values of maximum mean thrust coefficient at values of χ between $0.6 \sim 0.7$ instead of at $\chi \simeq 0.5$, as it is the case of the results provided solving the DNS in TUCAN. Moreover, it has to be commented that similarly to what occurred for the lift force, at $\chi = 0$ the generation of thrust is almost zero and for all the studied cases. Once again, these differences in the results is associated with the assumption made in the process of calculating the force components. Looking at figure 4.14 and figure 4.15, it is seen how while larger values of mean thrust coefficient respect to the expected ones are obtained, lower values of lift coefficient are achieved. Thus, a source of error in the orientation of the calculated components of the force respect to the actual ones estimated using TUCAN is expected.

In order to calculate the propulsive efficiency (equation 3.17) for each of the simulated cases, not only the components of the force are necessary but the moment of the airfoil at the LE. While solving the DNS in TUCAN the temporary history of data is provided for each one of the cases. Nevertheless, the simplified model has not been developed to calculate this moment yet. Since the work required to perform the pitching motion is much lower than the work required to perform the heaving one, and the moment at the leading edge is not the

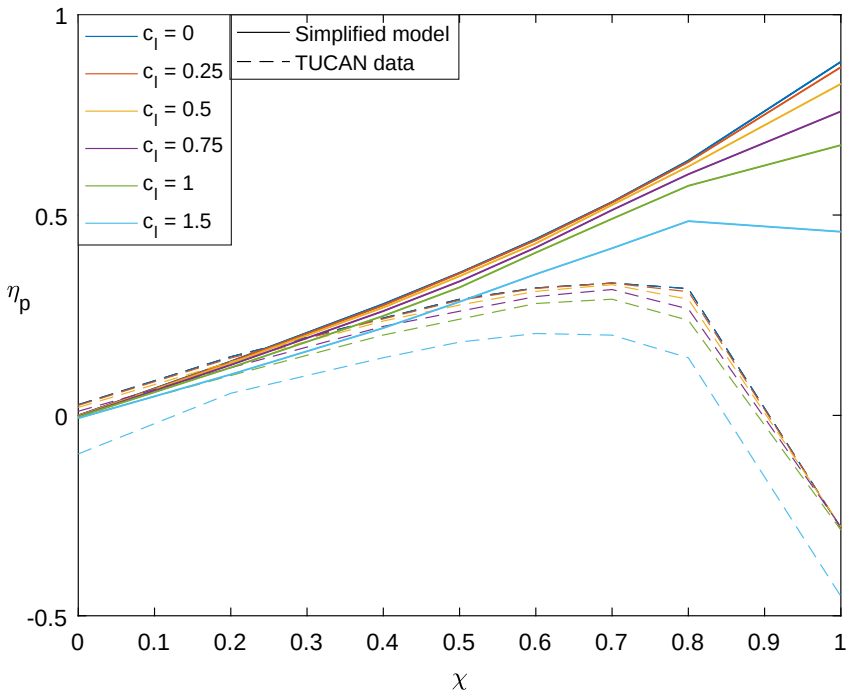

Figure 4.16: *Comparison of the propulsive efficiency (η_p) obtained using TUCAN and a simplified model for each one of the simulated cases.*

biggest contribution to the total moment computed at the quarter chord of the airfoil, using the data provided by TUCAN, it is considered that for those cases in which the work required for pitching is less than a 10% the work for heaving, the contribution of this term to the total moment can be neglected. After analyzing the data of the 48 different cases, it is seen how the criteria established is fulfilled in almost all the simulated cases except in some of the cases for $\bar{c}_l = 0$ (Cases with the nomenclature CXX000 collected in table 3.2). Thus, with this assumption a small source of error in the computation of the propulsive efficiency has to be added to the errors commented in the calculation of the components of the force. The results obtained using this simplified model are compared with the ones obtained using TUCAN in figure 4.16.

In said figure, it can be seen how despite the differences seen in the results concerning the aerodynamic forces, the propulsive efficiency calculated with the model, provide good results for low values of feathering parameter and after χ reaches a value of 0.5 the behaviour of the curves obtained for each target mean lift coefficient is completely different to the expected one. Once again the obtained results can be justify from the results previously obtained for the aerodynamic forces. It is seen how the effect of thrust force is higher than the lift one in the propulsive

efficiency. Thus, for small values of χ ($\chi < 0.4$) where the results of $\bar{c}_t$ are similar to the ones of TUCAN, good results are obtained in terms of η_p no matter the differences encountered in the results obtained for $\bar{c}_l$. Nevertheless, as the value of feathering parameter increases the values obtained for $\bar{c}_t$ are not so good, explaining the results obtained for η_p that continue being positive and even becomes bigger, and tends to infinity, for larger values of feathering parameter, behaviour that is explained due to the results obtained for the mean thrust coefficient.

Chapter 5

Regulatory framework and socioeconomic impact

One of the objectives of this project, is to be capable to predict the aerodynamic forces that take place under a flapping motion, with the purpose of using the obtained knowledge on improving the design of MAVs.

5.1 Regulatory framework

The interest put in micro aerial vehicles in the past years, and their huge variety of applications, has generated a controversy about their used, concretely about the restrictions of their used, and if it would be allowed to use them under any circumstance, in any place, by anyone and without restrictions of the aerial space. Although the debate is not solved, the possible regulations derived from it, do not affect to the implementation of the actual project in the design of MAVs, since the main purpose of the project is to increase the knowledge about the performance of insects and small bird to imitate their movements to design more efficient MAVs, and its implementation does not suppose a change on the structure, but a change on the parameters that affect to their kinematics without taking any safety risk for anyone (as it could be any modification on the structure of an aircraft). Moreover, a part from the possibility of implementing the acquired knowledge in their design, there is not any known regulation about the design and manufacturing of these vehicles.

5.2 Socioeconomic impact

As said before, one of the direct applications of the actual project is to improve the performance of MAVs in the new designed prototypes. In the past years MAVs have attracted the interest because of their huge variety of applications. These micro air vehicles, imitate the flight of small birds and insect, with dimensions lower than 15 cm that allow them to fly to remote, recondite, steep and hazardous places where aircraft or even drones can not access due to its bigger size. MAVs are

also provided with sensor to take measurements, photos, videos or take samples of water, air or terrain. Thus, their used in humanitarian, reconnaissance, rescue or military missions is more than attractive having a huge social impact. They could be used to test whether or not it is safe to breath the air under natural disasters as it is the case of a leakage at a nuclear power plant or the proximity of an active volcano, to detect if there is alive people in a landslide or an earthquake and to recognize the terrain in hazardous military missions allowing soldiers to avoid unnecessary risks.

Due to the huge variety of interesting applications, their use is more than ensure supposing a good rate of manufacturing, which would imply a positive economic impact and an advanced in technology.

Chapter 6

Summary and conclusions

6.1 Summary

This bachelor thesis aims to contribute in the understanding of the unsteady aerodynamics of flapping flights at low Reynolds number, which despite all the researching works made, are not completely understood yet due to its high complexity.

Along the execution of this project 48 different Direct Numerical Simulations have been launched in TUCAN, where an Immersed Boundary Method has been used to solve the Navier Stokes equations around an airfoil. With this project it is pretended to study the influence of feathering parameter in the unsteady aerodynamics of the flapping movement of a NACA 0012, at low Reynolds number and reduced frequency, and to achieve the best configuration of kinematic parameters to obtain maximum values of thrust and propulsive efficiency without penalizing the generation of lift.

To make this possible different values of feathering parameter in the range between 0 and 1, where propulsive forces takes place, are analyzed. At the beginning the selection of these values was made from 0.2 to 0.2, but in the process it was seen that $\chi = 0.5$ and $\chi = 0.7$ were values of interest in terms of thrust and propulsive efficiency, so that the final values studied were: 0, 0.2, 0.4, 0.5, 0.6, 0.7, 0.8 and 1. This values of feathering parameter were analyzed at 6 different values of lift coefficient (0, 0.25, 0.5, 0.75, 1 and 1.5) yielding in a total of 48 simulated cases. Due to the complexity of the problem and the amount of parameters involved, some of them have been fixed as it is the case of: Reynolds number, $Re = 500$; heaving amplitude , $h_0/c = 1$; pivoting point, $x_p = c/4$; phase shift between heaving and pitching motion, $\varphi = 90^o$ and reduced frequency, $k = 1.41$. To solved the equations of motion, the mean pitch angle and pitching amplitude were defined. Having fixed the rest of parameters θ_0 is directly obtained from the definition of χ and θ_m is varied continuously in an iterative process to achieve the desired values of lift coefficient.

6.2 Conclusions

While analyzing the results obtained in terms of maximum generated thrust and maximum propulsive efficiency, it has been seen that maximum values of thrust are obtained at $\chi \simeq 0.5$ and the ones of maximum propulsive efficiency are achieved at $\chi \simeq 0.7$. Since in this project, it is pretended to achieve a range of values of χ to optimize the performance of the airfoil, the exact values of feathering parameter for maximum propulsive efficiency and maximum generation of thrust have not been achieved performing DNS, since it would supposed an increased on the computational time and cost, that is out of the limits of the project. Thus, an estimation of the results that would be obtained performing a DNS in terms of $\bar{c_t}$ and η_p has been done for each one of the 6 different cases of mean lift coefficient. The results obtained are good enough to save said computational time. The error between the maximum obtained $\bar{c_t}$ and the one obtained performing the approximation is of 0.63 % for the case of $\bar{c_l} = 1$ and for the case of maximum propulsive efficiency this error is of 0.99% for the case of $\bar{c_l} = 1.5$. In order to achieve the best combination of parameters to compensate the generation of thrust and propulsive efficiency without penalizing the generation of lift it has been established that the best option is to flight at values of feathering parameters of $\chi \simeq 0.6$ achieving values of $\bar{c_l}$ slightly larger than 1.

Moreover, the analysis of the results of obtained in terms of aerodynamic forces and propulsive efficiency has been reinforced with a visualization of the flow for the most relevant cases, paying special attention to the effect caused by the LEV and TEV on the generation of this forces.

6.3 Future work

First of all, it has to be said that the results presented in this document can be taken into consideration as a reference for future works, where similar parameters are considered and the present project can be consider as a starting point for future works.

It could be interesting to increase the Reynolds number, since the one used in the simulation is a very low one. Nevertheless, it has to be considered that increasing Re more than approximately $Re = 3000$ can yield in some instabilities on the flow that would need a 3D DNS to be solved, which increases a lot the cost of the project. Thus, values of Re of 1000 or 2000 would be a good choice to see how the obtained results are modified. Moreover, an increase in Re would have and associate increase on the number of resolution points and the size of the computational box in order to achieve accurate results.

Looking at the results obtained in terms of aerodynamic forces and the procedure followed, it has been seen how for this project is not practical to continue

launching more simulations to achieve more precise values and an approximation is accurate enough. Nevertheless, introducing changes in the Re, and the size of the box it would be interesting to perform simulations for the most interesting cases in terms of maximum generation of thrust and propulsive efficiency taking as reference the results obtained by the approximated method used. Furthermore, it is recommended to perform some simulations at the interested points for some values of mean lift coefficient between 1 and 1.5, specially to see the results obtained in terms of generation of thrust.

Moreover, taking into account the results obtained in section 4.3, it could be interesting to check the values imposed for the translational and rotational constants at it supposed a big source of error in the results obtained, as well as the orientation of the forces that seems to be not the exact one. To finish with, although it represents a small source of error, and the final goal of this model is to achieve good results by means of simplifying the model proposed in Moriche 2017, it would be interesting to introduce the computation of moments in the model to improve the results in terms of propulsive efficiency.

Appendix A

Budget

An important part of any project, is the estimation of the total budget needed to develop it, in which the individual costs are broken down.

In the following lines, it can be found with detail, the most important items that take part in this project.

- **MATLAB license.**
  To postprocess the results obtained in the simulations, MATLAB has been used as a computational program. An academic license provided by the Univertisty has been used whose priced is value on 500 €.

- **Base computer.**
  To carry out the project a personal computer has been needed. A Toshiba laptop, intel-i7 provided with Microsoft Windows, has been used. Moreover, a remote-interface terminal to allow the shell remote conection in Linux has been indispensable. The cost of the computer is of 870 €.

- **Hours of engineering work.**
  To finish up the project, around 500 hours of work has been necesary. The price per work hour of a low experience engineering is estimated at 20 €/hour, yielding to a total of 10,000 €.

- **Software license.**
  The carry out the simulations the software used has been a CFD code developed at the bioengineering and aerospace department of UC3M. The estimated cost of the sofware is included in the budget by looking at the price of an equivalent software as it is the case of ANSYS FLUENT whose academic license is priced on around 6000 €.

- **Computational time.**
  Along the project 48 simulations have been performed, and between 15 and 22 hours per simulation have been needed before they converged. The simulations have been launched on a HPC cluster where 12 nodes per simulations have been used yielding in a total of 12000 cphours approximately. If the

computing hour is estimated in 0.2 €/hour acoording to CESGA, this adds 2.400 € to the total budget.

Table A.1 collects a summary of the neccesary cost to develop the project.

Subject	Price(€)
Software costs	8,900
Material costs	870
Engineering work	10,000
Total cost	**19,770**

Table A.1: *Summary of the project budget estimation.*

Appendix B

Flowchart and pseudocode

To better understand the postprocess of data explained in section 3.2.3 the flowchart and pseudocode are also included.

% Define $(\bar{c}_l, \theta_m)_{old}$ and $(\bar{c}_l, \theta_m)_{current}$
$\bar{c}_{l_{old}} = 0$;
$\theta_{m_{old}} = 0$;
$\bar{c}_{l_{target}} = 0.5$; % For the first case. Substitute according with the simulated case
$\theta_{m_{current}} = 3.81\pi/180$; % rad ($3.81^o$)

% Define number of steps, frequency, period and tolerances.
$n_{steps} = 2048$;
$k = 1.41$;
$T = 2\pi/k$;
$tol\_c_l = 1e-4$;
$tol\_\theta_m = 2\pi/3600$; % rad (0.1^o)
$tol\_error = 0.2$;%

% Launch the simulation in TUCAN until it finishes the execution and analyze the generated data.

Load data($F_x, F_y, time$)

If floor(time(end)/T)>= 2;

$c_l = -2 \cdot F_y$;

% Check if the simulation has converged

Calculate $\bar{c}_l$ for the first period: $\bar{c}_l(1) = mean(c_l(1 : n_{step}))$;

For i=2:floor(time(end)/T);

Calculate $\bar{c}_l$ for the next period: $\bar{c}_l(i) = mean(c_l(n_{step} \cdot (i-1) : n_{step} \cdot i))$;

If $|\bar{c}_l(i) - \bar{c}_l(i-1)| <= tol\_c_l$

disp(['The simulation has converged'])
$\bar{c}_{l_{current}} = \bar{c}_l(i)$;
Calculate the amplitude in signal (A):
$A = max(c_l(n_{step}(i-1) : n_{step}(i))) - min(c_l(n_{step}(i-1) : n_{step}(i)))$;

% Check if it has conclude
If $\left|\frac{\bar{c}_{l_{target}} - \bar{c}_{l_{current}}}{A}\right| > tol\_error$

disp(['The simulation has not conclude.'])
disp(['Apply the secant method'])
$\theta_{m_{root}} = \theta_{m_{current}} - \frac{\left(\bar{c}_{l_{current}} - \bar{c}_{l_{target}}\right)\left(\theta_{m_{current}} - \theta_{m_{old}}\right)}{\bar{c}_{l_{current}} - \bar{c}_{l_{old}}}$

% Check the diference between $\theta_{m_{root}}$ and $\theta_{m_{current}}$
If $|\theta_{m_{root}} - \theta_{m_{current}}| > tol\_\theta_m$

disp(['The simulation has not conclude'])
% Update variables
$\theta_{m_{old}} = \theta_{m_{current}}$;
$\theta_{m_{current}} = \theta_{m_{root}}$;
$\bar{c}_{l_{old}} = \bar{c}_{l_{current}}$;

Else
disp(['The simulation has conclude'])
End

Else
disp(['The simulation has conclude'])
End

Else
disp(['The simulation has not converged'])
End

End

Else
disp(['Launch again the simulation'])
End

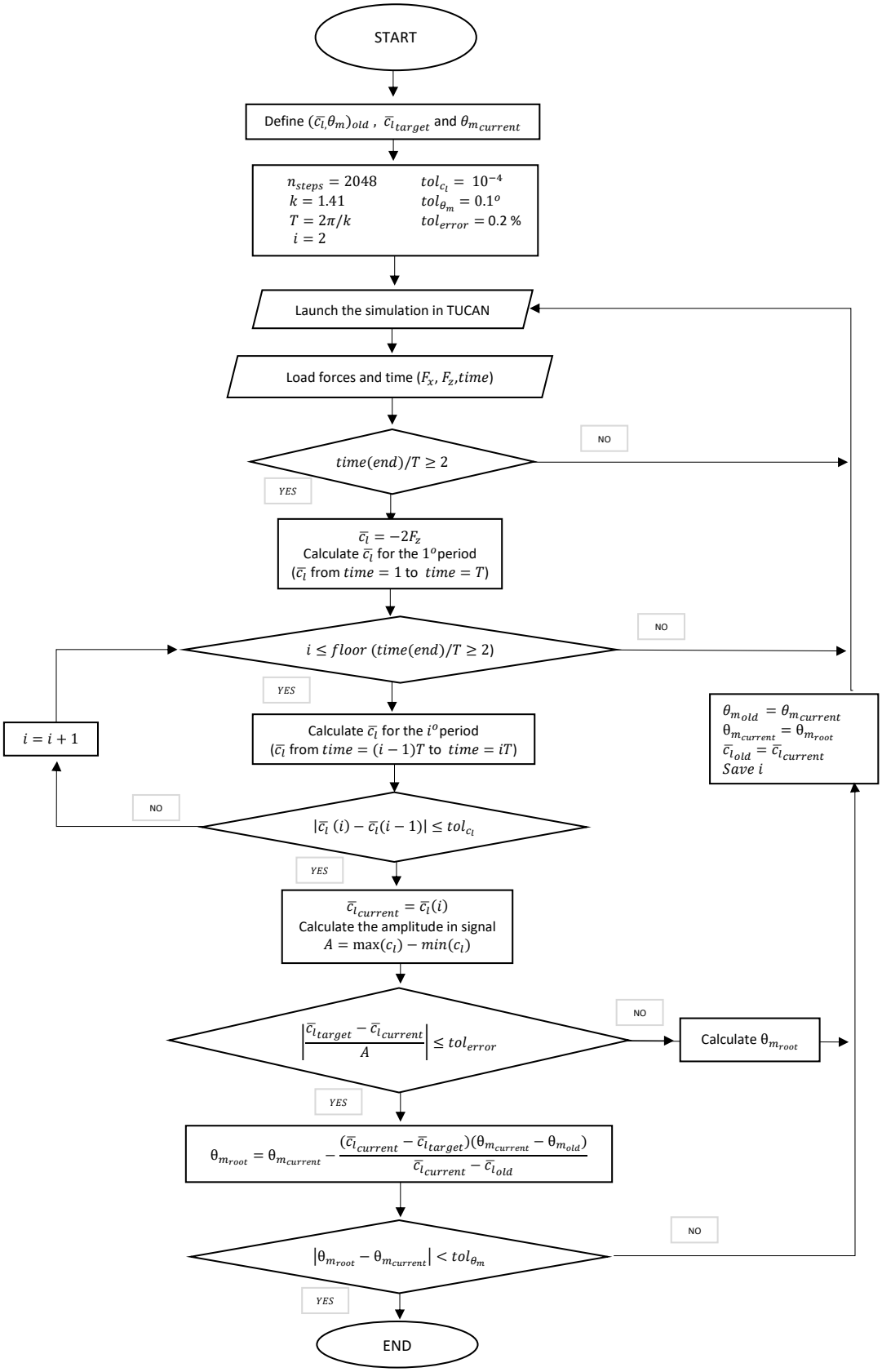
START
Define $(\bar{c}_l, \theta_m)_{old}$, $\bar{c}_{l_{target}}$ and $\theta_{m_{current}}$
$n_{steps} = 2048$
$k = 1.41$
$T = 2\pi/k$
$i = 2$
$tol_{c_l} = 10^{-4}$
$tol_{\theta_m} = 0.1^o$
$tol_{error} = 0.2\ \%$
Launch the simulation in TUCAN
Load forces and time (F_x, F_z,$time$)
$time(end)/T \geq 2$
NO
YES
$\bar{c}_l = -2F_z$
Calculate $\bar{c}_l$ for the 1^operiod
($\bar{c}_l$ from $time = 1$ to $time = T$)
$i \leq floor\ (time(end)/T \geq 2)$
NO
YES
$i = i + 1$
Calculate $\bar{c}_l$ for the i^operiod
($\bar{c}_l$ from $time = (i-1)T$ to $time = iT$)
$|\bar{c}_l\ (i) - \bar{c}_l(i-1)| \leq tol_{c_l}$
NO
YES
$\theta_{m_{old}} = \theta_{m_{current}}$
$\theta_{m_{current}} = \theta_{m_{root}}$
$\bar{c}_{l_{old}} = \bar{c}_{l_{current}}$
Save i
$\bar{c}_{l_{current}} = \bar{c}_l(i)$
Calculate the amplitude in signal
$A = \max(c_l) - min(c_l)$
$\left|\frac{\bar{c}_{l_{target}} - \bar{c}_{l_{current}}}{A}\right| \leq tol_{error}$
NO
Calculate $\theta_{m_{root}}$
YES
$\theta_{m_{root}} = \theta_{m_{current}} - \frac{(\bar{c}_{l_{current}} - \bar{c}_{l_{target}})(\theta_{m_{current}} - \theta_{m_{old}})}{\bar{c}_{l_{current}} - \bar{c}_{l_{old}}}$
$|\theta_{m_{root}} - \theta_{m_{current}}| < tol_{\theta_m}$
NO
YES
END

Bibliography

Anderson, JM et al. (1998). "Oscillating foils of high propulsive efficiency". In: *Journal of Fluid Mechanics* 360, pp. 41–72.

Ashraf, MA, J Young, and JCS Lai (2011). "Reynolds number, thickness and camber effects on flapping airfoil propulsion". In: *Journal of Fluids and structures* 27.2, pp. 145–160.

Baker, Allison H et al. (2012). "Scaling hypre's multigrid solvers to 100,000 cores". In: *High-Performance Scientific Computing*. Springer, pp. 261–279.

Betz, Albert (1912). "Ein beitrag zur erklaerung des segelfluges". In: *Zeitschrift fur Flugtechnik und Motorluftschiffahrt* 3.1, pp. 269–272.

Brown, David L, Ricardo Cortez, and Michael L Minion (2001). "Accurate projection methods for the incompressible Navier–Stokes equations". In: *Journal of computational physics* 168.2, pp. 464–499.

Carr, LAWRENCEW (1988). "Progress in analysis and prediction of dynamic stall". In: *Journal of aircraft* 25.1, pp. 6–17.

Chang, Chien-Cheng (1992). "Potential flow and forces for incompressible viscous flow". In: *Proceedings of the Royal Society of London A: Mathematical, Physical and Engineering Sciences*. Vol. 437. 1901. The Royal Society, pp. 517–525.

Dagum, Leonardo and Ramesh Menon (1998). "OpenMP: an industry standard API for shared-memory programming". In: *IEEE computational science and engineering* 5.1, pp. 46–55.

Dickinson, Michael H, Fritz-Olaf Lehmann, and Sanjay P Sane (1999). "Wing rotation and the aerodynamic basis of insect flight". In: *Science* 284.5422, pp. 1954–1960.

Ellington, Charles P et al. (1996). "Leading-edge vortices in insect flight". In: *Nature* 384.6610, p. 626.

Fenercioglu, Idil and Oksan Cetiner (2012). "Categorization of flow structures around a pitching and plunging airfoil". In: *Journal of Fluids and Structures* 31, pp. 92–102.

Ferziger, Joel H and Milovan Peric (2012). *Computational methods for fluid dynamics*. Springer Science & Business Media.

Ford, CW Pitt and Holger Babinsky (2013). "Lift and the leading-edge vortex". In: *Journal of Fluid Mechanics* 720, pp. 280–313.

Forum, Message P. (1994). *Mpi: A message-passing interface standard*. Tech. rep. Knoxville, TN, USA.

Freymuth, Peter (1988). "Propulsive vortical signature of plunging and pitching airfoils". In: *AIAA journal* 26.7.

Garrick, IE (1937). "Propulsion of a flapping and oscillating airfoil". In:

Glauert, H (1930). "The force and moment on an oscillating aerofoil". In: *Vorträge aus dem Gebiete der Aerodynamik und verwandter Gebiete*. Springer, pp. 88–95.

Group, HDF et al. (2016). "Hierarchical Data Format, version 5, 1997–2016". In: *URL: http://www. hdfgroup. org/HDF5*.

Heathcote, Sam, Z Wang, and Ismet Gursul (2008). "Effect of spanwise flexibility on flapping wing propulsion". In: *Journal of Fluids and Structures* 24.2, pp. 183–199.

"High performance preconditioners" (2016 June). In: *URL: http://www.llnl.gov/CaSA/hypre/*.

Isogai, K, Y Shinmoto, and Y Watanabe (1999). "Effects of dynamic stall on propulsive efficiency and thrust of flapping airfoil". In: *AIAA journal* 37.10, pp. 1145–1151.

Jones, KD and MF Platzer (1997). "Numerical computation of flapping-wing propulsion and power extraction". In: *AIAA paper* 97, p. 826.

Katzmayr, Richard (1922). "Effect of periodic changes of angle of attack on behavior of airfoils". In:

Knoller, Richard (1909). *Die gesetze des luftwiderstandes*. Verlag des Österreichischer Flugtechnischen Vereines.

Koochesfahani, Manoochehr M (1989). "Vortical patterns in the wake of an oscillating airfoil". In: *AIAA journal* 27.9, pp. 1200–1205.

Lai, JCS and MF Platzer (1999). "Jet characteristics of a plunging airfoil". In: *AIAA journal* 37.12, pp. 1529–1537.

Lewin, Gregory C and Hossein Haj-Hariri (2003). "Modelling thrust generation of a two-dimensional heaving airfoil in a viscous flow". In: *Journal of Fluid Mechanics* 492, pp. 339–362.

Lua, KB et al. (2007). "Wake-structure formation of a heaving two-dimensional elliptic airfoil". In: *AIAA journal* 45.7, p. 1571.

Martín-Alcántara, A, R Fernandez-Feria, and E Sanmiguel-Rojas (2015). "Vortex flow structures and interactions for the optimum thrust efficiency of a heaving airfoil at different mean angles of attack". In: *Physics of Fluids* 27.7, p. 073602.

McCroskey, William J (1982). "Unsteady airfoils". In: *Annual review of fluid mechanics* 14.1, pp. 285–311.

Mittal, Rajat and Gianluca Iaccarino (2005). "Immersed boundary methods". In: *Annu. Rev. Fluid Mech.* 37, pp. 239–261.

Moriche, Manuel (2017). "A numerical study on the aerodynamic forces and the wake stability of flapping flight at low Reynolds number". PhD thesis. Universidad Carlos III de Madrid.

— (2016). "Private communication". In:

Pesavento, Umberto and Z Jane Wang (2004). "Falling paper: Navier-Stokes solutions, model of fluid forces, and center of mass elevation". In: *Physical review letters* 93.14, p. 144501.

Peskin, Charles S (2002). "The immersed boundary method". In: *Acta numerica* 11, pp. 479–517.

Roma, Alexandre M, Charles S Peskin, and Marsha J Berger (1999). "An adaptive version of the immersed boundary method". In: *Journal of computational physics* 153.2, pp. 509–534.

Sane, Sanjay P (2003). "The aerodynamics of insect flight". In: *Journal of experimental biology* 206.23, pp. 4191–4208.

Shyy, Wei et al. (2013). *An introduction to flapping wing aerodynamics*. Vol. 37. Cambridge University Press.

Theodorsen, Theodore and WH Mutchler (1935). "General theory of aerodynamic instability and the mechanism of flutter". In:

Triantafyllou, GS, MS Triantafyllou, and MA Grosenbaugh (1993). "Optimal thrust development in oscillating foils with application to fish propulsion". In: *Journal of Fluids and Structures* 7.2, pp. 205–224.

Uhlmann, Markus (2005). "An immersed boundary method with direct forcing for the simulation of particulate flows". In: *Journal of Computational Physics* 209.2, pp. 448–476.

Walker, J, H Helin, and D Chou (1985). *Unsteady surface pressure measurements on a pitching airfoil*. Tech. rep. FRANK J SEILER RESEARCH LAB UNITED STATES AIR FORCE ACADEMY CO.

Wang, Z Jane (2000). "Vortex shedding and frequency selection in flapping flight". In: *Journal of Fluid Mechanics* 410, pp. 323–341.

Widmann, A and C Tropea (2015). "Parameters influencing vortex growth and detachment on unsteady aerodynamic profiles". In: *Journal of Fluid Mechanics* 773, pp. 432–459.

Young, John and JCS Lai (2004). "Oscillation frequency and amplitude effects on the wake of a plunging airfoil". In: *AIAA journal* 42.10, pp. 2042–2052.

Yuste, Sergio Redondo (2017). "Validation of a semi-analytic force model for flapping flight at low Reynolds number". MA thesis. Universidad Carlos III de Madrid.